RICE UNIVERSITY

Refined Spectral Asymptotics for the Telegrapher's Equation

by

Sharmaine Jennings

A Thesis Submitted
in Partial Fulfillment of the
Requirements for the Degree

Master of Arts

Approved, Thesis Committee:

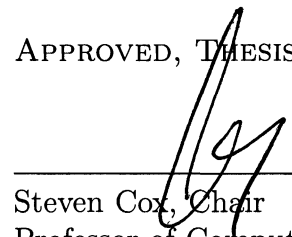

Steven Cox, Chair
Professor of Computational and Applied Mathematics

Mark Embree
Professor of Computational and Applied Mathematics

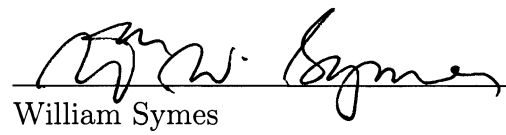

William Symes
Noah G. Harding Professor of
Computational and Applied Mathematics

Houston, Texas

April, 2011

ABSTRACT

Refined Spectral Asymptotics for the Telegrapher's Equation

by

Sharmaine Jennings

In this research, I derive a refined asymptotic expression for the eigenvalues, $\{\lambda_n\}_{n\in\mathbb{Z}}$, of the operator matrix from the telegrapher's equation to accuracy $O(1/n^2)$. First, the expression for the "shooting function" is refined to $O(1/n^2)$ using a "fake potential" and a Neumann series. Then, this expression for the "shooting function" is used to refine the expressions for the eigenvalues. This refinement of the previously published results of accuracy $O(1/|n|)$ enables the inverse spectral problem (recovering unknown resistance) to be solved in numerical experiments, using Fourier series. One application of this recovery process would be to find a fault in the insulation of a submarine telegraph cable without having to physically inspect every inch of the cable.

Acknowledgements

There are many individuals I wish to thank for helping me in writing this thesis. First, I want to acknowledge the guidance of my advisors, Dr. Cox and Dr. Embree, without whose help I could not have finished this thesis on time. I would also like to acknowledge the help given to me by my friends in the CAAM department and other departments at Rice University. Also, I want to take this opportunity to thank my family for their support through this process. Lastly, I want to thank my Heavenly Father for His guidance during this part of my journey - without Him I can do nothing.

Contents

Illustrations

Tables

Chapter 1

Introduction

In this research, I derive a refined asymptotic expression for the eigenvalues, $\{\lambda_n\}_{n\in\mathbb{Z}}$, of the operator matrix from the telegrapher's equation to accuracy $O(1/n^2)$. First, the expression for the "shooting function" is refined to $O(1/n^2)$ using a "fake potential," a Volterra integral of the second kind, and a Neumann series. Then, this expression for the "shooting function" is used to refine the expressions for the eigenvalues. This refinement of the previously published results of accuracy $O(1/|n|)$ by Cox and Knobel [4] enables the inverse spectral problem (recovering unknown resistance) to be solved in numerical experiments, using Fourier series, similar to the results Cox and Embree [3] were able to recover from the damped wave equation. One application of being able to recover unknown resistance in the telegrapher's equation would be to find a fault in the insulation of a submarine telegraph cable without having to physically inspect every inch of the cable, as illustrated in Chapter 6.

The goal of this research is to find a way to recover unknown resistance functions from spectral data in the telegrapher's equation, a hyperbolic partial differential equation. First, the derivation and a short history of the telegrapher's equation will be described.

1.1 Derivation of the Telegrapher's Equations

A diagram of a small piece of telegraph wire is seen in Figure 1.1. The model consists of two conducting lines, parallel to each other, which together make a transmission line.

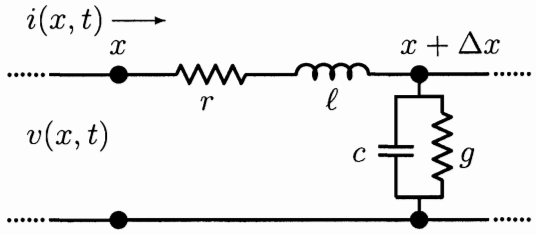

Figure 1.1 : Model of a transmission line.

Let x be the distance along a transmission line, t be time, $v(x,t)$ be the potential difference, or voltage, between the two conductors in the transmission line, and $i(x,t)$ be the current in the "live" conductor. Let $r(x)$ be the resistance per unit length and $g(x)$ be the leakage conductance per unit length. The general model also includes $\ell(x)$, the inductance per unit length, and $c(x)$, the capacitance per unit length.

The voltage change across this length of transmission line is given by

$$v(x+\Delta x,t) - v(x,t) = -r(x)i(x,t)\Delta x - \ell(x)i_t(x,t)\Delta x$$

because of the resistance, $r(x)$, along the "live" conductor and the inductance coil. The amount of current that escapes from the "live" conductor is

$$i(x+\Delta x,t) - i(x,t) = -g(x)v(x,t)\Delta x - c(x)v_t(x,t)\Delta x$$

because of the resistance, $g(x)$, and capacitance. Dividing these equations by Δx and

taking the limit as Δx goes to zero results in the telegrapher's equation,

$$-\ell(x)i_t(x,t) = v_x(x,t) + r(x)i(x,t) \tag{1.1}$$
$$-c(x)v_t(x,t) = i_x(x,t) + g(x)v(x,t).$$

For simplicity, assume the line is of unit length. In this research, $\ell(x)$ and $c(x)$ are assumed to be a constant value of one, because only $r(x)$ and $g(x)$ contribute to the weakening in $v(x,t)$. Under these assumptions and if

$$u(x,t) \equiv \begin{pmatrix} u_1(x,t) \\ u_2(x,t) \end{pmatrix} = \begin{pmatrix} i(x,t) \\ v(x,t) \end{pmatrix}, \tag{1.2}$$

then (1.1) can be written as

$$-u_t = \mathcal{A}(P)u \tag{1.3}$$

where

$$\mathcal{A}(P)u \equiv B\partial_x u + Pu, \quad B = \begin{pmatrix} 0 & 1 \\ 1 & 0 \end{pmatrix}, \quad \text{and} \quad P(x) = \begin{pmatrix} r(x) & 0 \\ 0 & g(x) \end{pmatrix}.$$

This research considers two different pairs of boundary conditions, one with homogeneous Dirichlet conditions on v at both ends,

$$v(0,t) = v(1,t) = 0,$$

which corresponds to the transmission line being grounded at both ends, and the other with homogeneous Dirichlet conditions on the left end of v and the right end of i,

$$v(0,t) = i(1,t) = 0.$$

These boundary conditions are chosen because they provide useful spectral data to recover unknown r and g. This problem is posed in the Hilbert space $L^2(0,1) \times$

$L^2(0,1)$. $\mathcal{A}(P)$ operates in the domains

$$D_k = \{u \in H^1(0,1)^2 : W_0 u(0) + W_k u(1) = 0\}, \quad k = 1, 2,$$

where

$$W_0 = \begin{pmatrix} 0 & 1 \\ 0 & 0 \end{pmatrix}, \quad W_1 = \begin{pmatrix} 0 & 0 \\ 0 & 1 \end{pmatrix}, \quad \text{and} \quad W_2 = \begin{pmatrix} 0 & 0 \\ 1 & 0 \end{pmatrix}.$$

Following the notation of Cox and Knobel [4], let $\mathcal{A}_k(P)$ denote the operator $\mathcal{A}(P)$ on domain D_k.

1.2 History of the Telegrapher's Equation

When the line is assumed to be uniform and r and g are also assumed to be constant, it is possible to arrive at the "classical telegrapher's equation,"

$$\ell c v_{tt}(x,t) - v_{xx}(x,t) + (rc + \ell g) v_t(x,t) + rgv(x,t) = 0. \tag{1.4}$$

However, the model was not always known to have this form.

In 1855, Sir William Thompson (Lord Kelvin) published his model to describe the electrical properties of a telegraph line submerged in water, with some leakage of voltage through the insulation to the water [15, p. 387]. When his model is compared to (1.4), it can be seen that he assumes the coefficient of $v_{tt}(x,t)$ to be zero even though Faraday had already published results stating that the kind of cables Lord Kelvin was investigating had measurable inductance when used in water, as opposed to air [9, p. 258]. In 1857, Kirchhoff first published the telegrapher's equation in the form of (1.4) [9, p. 133].

Until the 1850s, the work being done with the telegrapher's equation was in perfecting the mathematical model to accurately predict and describe the physical behavior observed in the telegraph wires. The next step in the analysis of the telegrapher's

equation that is important to this research was finding the eigenvalues and eigenvectors of related problems.

1.3 Forward and Inverse Problems

The eigenvalue problem for (1.3) is to find $u \neq 0, u \in D_k$ such that

$$\mathcal{A}_k(P)u = \lambda u. \tag{1.5}$$

The problem of finding the eigenvalues, $\{\lambda_n(P)\}_{n\in\mathbb{Z}}$, and eigenvectors when r, g, and boundary conditions are given is regarded as the *forward problem.*

In his book published in 1877, Lord Rayleigh studied the frequencies of vibration of strings when the density was not necessarily constant, a type of *forward problem*, and first proposed the idea of determining the density of a string when the frequencies of vibration were known, a type of *inverse problem* [1].

Determining if a given set of eigenvalues corresponds to a particular set of coefficients, r, g, c, and ℓ, and boundary conditions, which is an *inverse spectral problem* is the subsequent step in the progression of the analysis of the telegrapher's equation [17].

A great deal of analysis has been done on the inverse spectral problem for the Sturm-Liouville equation

$$-\frac{d^2}{dx^2}u(x) + p(x)u(x) = \lambda u(x), \tag{1.6}$$

[12, 17]. When boundary conditions are included with (1.6), it is known that p in (1.6) can be completely determined by two spectra [17]. Considering the Sturm-Liouville equation is important because some of the results from the Sturm-Liouville equation can be applied to other equations, including the telegrapher's equation [17].

For example, Yamamoto extends two uniqueness theorems for the Sturm-Liouville equation to a more general form of (1.5) under certain boundary conditions [17].

Less work has been done for problems like (1.5) than for the Sturm-Liouville equation [17]. Yamamoto, when analyzing his more general form of (1.5), addresses under what conditions a spectrum determines unique coefficients and boundary conditions and observes that one set of boundary conditions will not be enough to determine both coefficients, r and g [17]. This fact is important in this thesis in trying to recover unknown resistance, r and/or g, in the telegrapher's equation.

The telegrapher's equation is closely related to the wave equation with viscous damping, which can be obtained from (1.3) in the case that r is zero, and both are special cases of the equation studied by Yamamoto. Cox and Zuazua analyzed the damped wave equation and derived an asymptotic expression for the eigenvalues of the operator to accuracy $O(1/|n|)$ [5]. Cox and Embree extended this asymptotic expression for the eigenvalues of the operator to accuracy $O(1/n^2)$, and this information is used to recover the even damping function from a given spectrum in numerical experiments [3]. This leads me to believe recovering information about resistance in the telegrapher's equation is possible after a similar refinement of the expression for the eigenvalues.

Returning to the telegrapher's equation, Cox and Knobel derived an asymptotic expression for the eigenvalues of the operator $\mathcal{A}(P)$ to accuracy $O(1/|n|)$ [4].

In this thesis, I refine the asymptotic expression for the eigenvalues of the operator, $\mathcal{A}(P)$, to accuracy $O(1/n^2)$ from the expression published by Cox and Knobel, using a "fake potential" and a Neumann series. These improved estimates are important because they prove useful in solving inverse spectral problems in numerical experiments, using Fourier series. In Chapter 6 of this thesis, several examples of

numerical results are presented in which a specific combination of r and g can be recovered using the refined asymptotic expression.

1.4 Applications

One straightforward application of improved asymptotic expressions for the eigenvalues of $\mathcal{A}(P)$ could apply to a submarine telegraph cable, such as the transatlantic cable. If errors were seen in transmissions and it was suspected these errors were caused by a problem in the insulation of the cable, it would be extremely costly to examine every inch of the cable in an attempt to find the fault. However, with the improved asymptotic expressions, information about the eigenvalues could be measured at the end of the damaged cable, which are easily accessible, and the information used to solve the inverse problem for r and/or g to find the fault in the cable.

Studying the telegrapher's equation is not only interesting for historical sake or because it involves an incremental increase in difficulty over other problems; the telegrapher's equation is used to model other physical phenomena besides electricity being sent through telegraph wires. In fact, even though in modern communications most transmissions are "wireless," if the length of the wire connecting the antenna or transmitter is longer than $1/8$ of the wave being transmitted, then the telegrapher's equation applies [10].

With some minor changes, the telegrapher's equation is also used to model the circulatory system, and an example is shown in Figure 1.2 [2]. Instead of voltage and current, in this application, the telegrapher's equation models pressure and volumentric flow, respectively [7]. In this application, the coefficients r, ℓ, c, and g now correspond to "resistance, inertance, arterial compliance, and resistance due to arterial wall viscosity, respectively" [8, p. 46]. Leung et al. published some results

using the telegrapher's equation to determine arterial stiffness (which, if determined accurately, could aid doctors in being able to diagnose various vascular diseases) in patients from various measurements taken, none of which require incisions [7]. Mainardi et al. published a study estimating the "vascular input impedance" in the brachial artery utilizing the telegrapher's equation as a model, also using measurements that did not require incisions [11]. Improvements in being able to recover the coefficients of the telegrapher's equation could lead to increased applicability of the telegrapher's equation to modeling properties of the circulatory system and other fields of study.

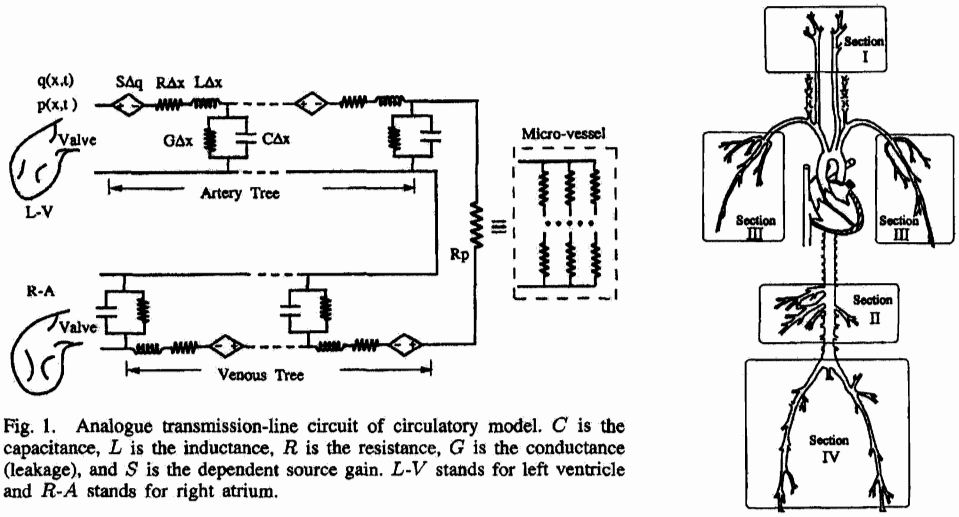

Fig. 1. Analogue transmission-line circuit of circulatory model. C is the capacitance, L is the inductance, R is the resistance, G is the conductance (leakage), and S is the dependent source gain. L-V stands for left ventricle and R-A stands for right atrium.

Figure 1.2 : Modeling the circulatory system with the telegrapher's equation [2].

In Chapter 2 of this thesis, the expressions for the eigenvalues and eigenvectors of the operator matrix are derived for constant r and g. These expressions form the basis of the refined expression for the eigenvalues. The refinement of the expression for the eigenvalues of $\mathcal{A}_1(P)$ is given in some detail in Chapter 3. The refinement of the eigenvalues of $\mathcal{A}_2(P)$ is almost exactly the same and is given, with much less detail, in Chapter 4. In Chapter 5, the procedure for using the refined expression

for the eigenvalues of $\mathcal{A}_1(P)$ to solve the inverse spectral problem is described. The results obtained from invoking this recovery procedure on a variety of r and g are presented in Chapter 6. The numerical methods used to calculate the eigenvalues of $\mathcal{A}_k(P)$ in MATLAB which are used in the inverse spectral problem are described in Chapter 7.

Chapter 2

Eigenvalues and Eigenvectors for constant r and g

Before finding asymptotic expressions for the eigenvalues and eigenvectors of $\mathcal{A}(P)$, the eigenvalues and eigenvectors of the telegrapher's equation with constant coefficients will be derived in this chapter. If $r(x) = r_0$ and $g(x) = g_0$, the eigenvalue problem $\mathcal{A}(P_0)u = \lambda u$ can be written as

$$\begin{pmatrix} v'(x) \\ i'(x) \end{pmatrix} = \begin{pmatrix} (\lambda - r_0)i(x) \\ (\lambda - g_0)v(x) \end{pmatrix}. \tag{2.1}$$

Taking the derivative with respect to x of the first line of (2.1) gives

$$v''(x) = (\lambda - r_0)i'(x). \tag{2.2}$$

Substituting the second line of (2.1) into (2.2) gives

$$v''(x) = (\lambda - r_0)(\lambda - g_0)v(x). \tag{2.3}$$

This equation has the general solution

$$v(x) = \alpha \cosh\left(x\sqrt{(\lambda - r_0)(\lambda - g_0)}\right) + \beta \sinh\left(x\sqrt{(\lambda - r_0)(\lambda - g_0)}\right) \tag{2.4}$$

for constants α and β.

2.1 $\mathcal{A}_1$: Dirichlet Boundary Conditions

To find the eigenvalues, λ_n, of $\mathcal{A}_1(P_0)$, first substituting $v(0) = 0$ into (2.4) gives $\alpha = 0$. Then, substituting $v(1) = 0$ into $v(x) = \beta \sinh\left(x\sqrt{(\lambda - r_0)(\lambda - g_0)}\right)$ gives

$\sinh\left(\sqrt{(\lambda - r_0)(\lambda - g_0)}\right) = 0$, which is true when

$$\sqrt{(\lambda_n - r_0)(\lambda_n - g_0)} = in\pi, \quad n \in \mathbb{Z}. \tag{2.5}$$

Therefore,

$$\lambda_{\pm n} = \frac{1}{2}\left(r_0 + g_0 \pm \sqrt{(r_0 - g_0)^2 - 4n^2\pi^2}\right) \tag{2.6}$$

are the eigenvalues for $\mathcal{A}_1(P_0)$.

To aid in the analysis in later chapters, it will be helpful to define a *simple* matrix as a matrix, P_0, that has no repeated eigenvalues (r_0 and g_0 are such that $(r_0 - g_0)^2 \neq 4n^2\pi^2$ for any $n \in \mathbb{Z}$).

In Figure 2.1, eigenvalues of $\mathcal{A}_1(P_0)$ are plotted for various r_0 when $g_0 = 2$ to illustrate the behavior of the eigenvalues. These eigenvalues were calculated with spectral discretization using $N = 128$ using the method described in Chapter 7. One behavior to notice is when $r_0 - g_0$ is large enough, some complex eigenvalues become pure real eigenvalues, which can be seen in the plot when $r_0 = 8.4$. It is also important to notice that as r_0 increases (in the plot, from 1 to 8.4), the real part of these eigenvalues travels to the right in the complex plane. Similar behavior would be seen in graphs if only g_0 were increased or if both r_0 and g_0 were increased. So, by taking $r_0 = g_0$ sufficiently large, all eigenvalues can be made to have real part as close to infinity as is desired, with only one real eigenvalue.

The eigenvalue expression in (2.6) can also be written in asymptotic form as

$$\begin{aligned}\lambda_{\pm n} &= \frac{1}{2}\left[r_0 + g_0 \pm i\left(2n\pi - \frac{(r_0 - g_0)^2}{4n\pi}\right) + O\left(\frac{1}{n^3}\right)\right] \\ &= \frac{r_0 + g_0}{2} \pm i\left(n\pi - \frac{(r_0 - g_0)^2}{8n\pi}\right) + O\left(\frac{1}{n^3}\right).\end{aligned} \tag{2.7}$$

This form will be used in the next chapter.

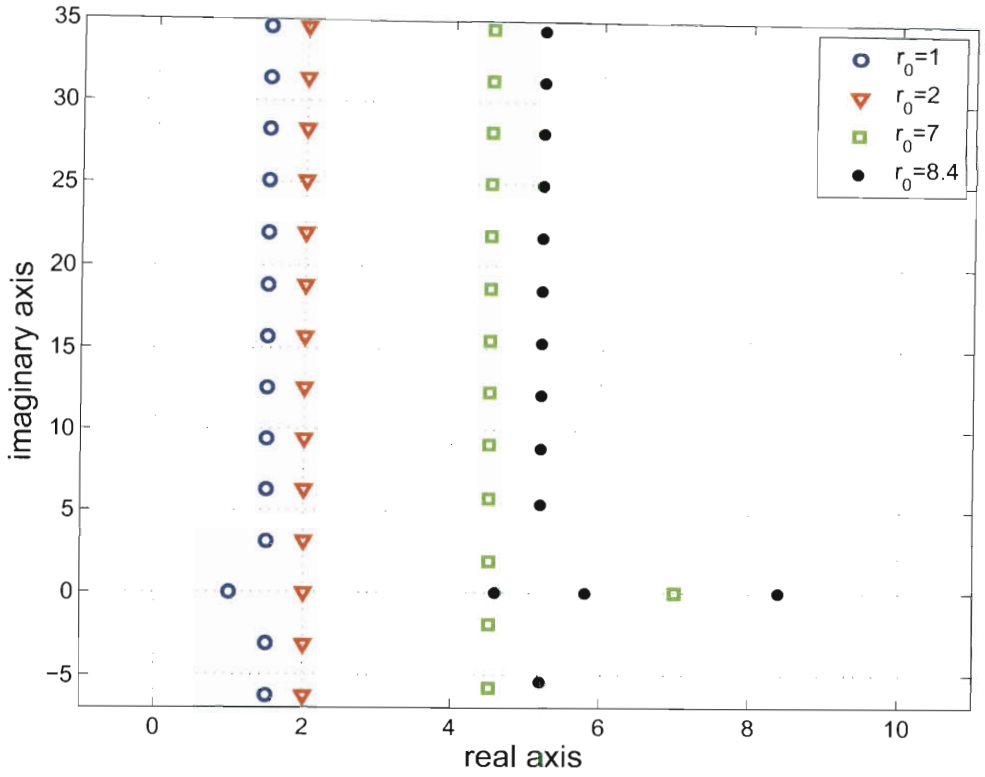

Figure 2.1 : The eigenvalues of $\mathcal{A}_1(P_0)$ for $g_0 = 2$ and various values of r_0. As r_0 increases, the spectrum moves to the right, and when $r_0 - g_0$ is large enough, some complex eigenvalues become pure real eigenvalues.

The eigenfunctions for v corresponding to (2.6) are

$$v_n(x) = \sinh(in\pi x) = i\sin(n\pi x). \tag{2.8}$$

Referring back to (2.1) to find $i_n(x)$, $v'(x) = (\lambda - r_0)i(x)$, so

$$i_n(x) = \frac{v_n'(x)}{\lambda_n - r_0} = \frac{in\pi\cos(n\pi x)}{\lambda_n - r_0}. \tag{2.9}$$

Therefore, the eigenvector corresponding to (2.6) is

$$\begin{pmatrix} i_n(x) \\ v_n(x) \end{pmatrix} = \begin{pmatrix} \frac{in\pi}{\lambda_n - r_0}\cos(n\pi x) \\ i\sin(n\pi x) \end{pmatrix}. \tag{2.10}$$

Here, zero is allowed as an eigenvalue because (2.10) would not be the zero vector when $n = 0$.

Figure 2.2 shows the graphs of the first few eigenvectors for $\mathcal{A}_1(P_0)$ when $r(x) = 8.4$ and $g(x) = 2$. (These eigenvectors were calculated by the same method as described for the eigenvalues.)

When $r(x) = 0$ and $g(x) = 0$, the expressions in (2.6) and (2.10) simplify to

$$\lambda_n = in\pi, \quad n \in \mathbb{Z} \tag{2.11}$$

and

$$\begin{pmatrix} i_n(x) \\ v_n(x) \end{pmatrix} = \begin{pmatrix} \cosh(in\pi x) \\ \sinh(in\pi x) \end{pmatrix} = \begin{pmatrix} \cos(n\pi x) \\ i\sin(n\pi x) \end{pmatrix}. \tag{2.12}$$

2.2 $\mathcal{A}_2$: Mixed Boundary Conditions

To find the eigenvalues, μ_n, of $\mathcal{A}_2(P_0)$, again substituting $v(0) = 0$ into (2.4) gives $\alpha = 0$.

From the first line in (2.1), if $i(1) = 0$, then $v'(1) = 0$. Combining $v(x) = \beta \sinh\left(x\sqrt{(\mu - r_0)(\mu - g_0)}\right)$ and $v'(1) = 0$ gives

$$v'(1) = \beta\sqrt{(\mu - r_0)(\mu - g_0)}\cosh\left(\sqrt{(\mu - r_0)(\mu - g_0)}\right) = 0,$$

which is true when

$$\sqrt{(\mu_n - r_0)(\mu_n - g_0)} = \frac{i(2n+1)\pi}{2}, \quad n \in \mathbb{Z}.$$

Therefore,

$$\mu_{\pm n} = \frac{1}{2}\left(r_0 + g_0 \pm \sqrt{(r_0 - g_0)^2 - \pi^2(2n+1)^2}\right) \tag{2.13}$$

are the eigenvalues of $\mathcal{A}_2(P_0)$. This expression can be written in asymptotic form as

$$\mu_{\pm n} = \frac{r_0 + g_0}{2} \pm i\left(\frac{(2n+1)\pi}{2} - \frac{(r_0 - g_0)^2}{(8n+4)\pi}\right) + O\left(\frac{1}{n^3}\right). \tag{2.14}$$

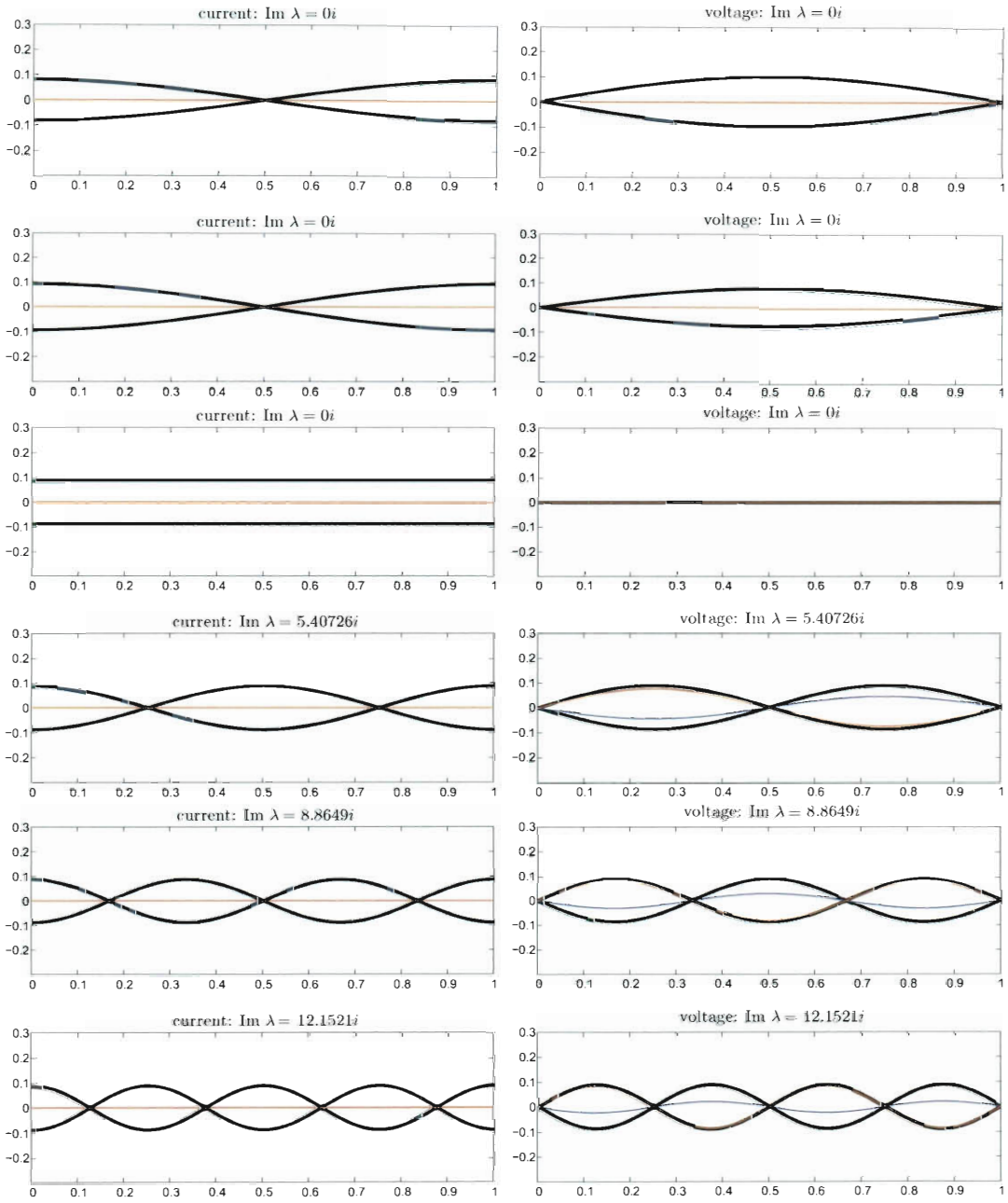

Figure 2.2 : The first few eigenvectors of $\mathcal{A}_1(P_0)$ for $g_0 = 2$ and $r_0 = 8.4$. The blue curve is the real part of the eigenfunction, and the red curve is the imaginary part of the eigenfunction. The black curves are the positive and negative absolute value of the eigenfunction.

This form will be used in Chapter 4.

In Figure 2.3, eigenvalues of $\mathcal{A}_2(P_0)$ are plotted for various r_0 when $g_0 = 2$. Similar behavior is seen, as in the previous section, of complex eigenvalues becoming real as $r_0 - g_0$ becomes large enough, and as r_0 increases, the spectrum, again, moves to the right. The main differences between the eigenvalues of $\mathcal{A}_1(P_0)$ and $\mathcal{A}_2(P_0)$ are in the imaginary part.

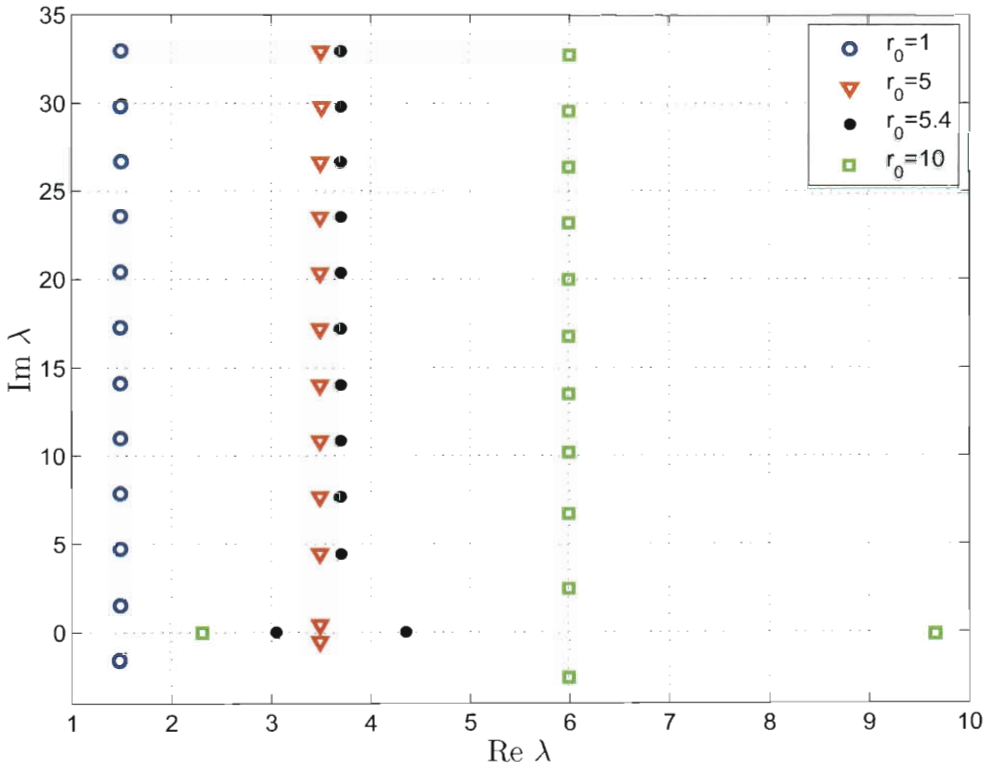

Figure 2.3 : The eigenvalues of $\mathcal{A}_2(P_0)$ for $g_0 = 2$ and various values of r_0. As r_0 increases, the spectrum moves to the right, and when $r_0 - g_0$ is large enough, some complex eigenvalues become pure real eigenvalues.

The eigenfunctions for v corresponding to (2.13) are

$$v_n(x) = \sinh\left(\frac{i(2n+1)\pi x}{2}\right) = i\sin\left(\frac{(2n+1)\pi x}{2}\right). \tag{2.15}$$

Referring back to (2.1) to find $i_n(x)$, $v'(x) = (\mu - r_0)i(x)$, so

$$i_n(x) = \frac{v_n'(x)}{\mu_n - r_0} = \frac{i(2n+1)\pi}{2(\mu_n - r_0)} \cos\left(\frac{(2n+1)\pi x}{2}\right). \tag{2.16}$$

Therefore, the eigenvector corresponding to (2.13) is

$$\begin{pmatrix} i_n(x) \\ v_n(x) \end{pmatrix} = \begin{pmatrix} \frac{i(2n+1)\pi}{2(\mu_n - r_0)} \cos\left(\frac{(2n+1)\pi x}{2}\right) \\ i \sin\left(\frac{(2n+1)\pi x}{2}\right) \end{pmatrix}. \tag{2.17}$$

Figure 2.4 shows the graphs of the first few eigenvectors for $\mathcal{A}_2(P_0)$ when $r(x) = 10$ and $g(x) = 2$.

If $r(x) = 0$ and $g(x) = 0$, the expressions in (2.13) and (2.17) simplify to

$$\mu_n = \frac{1}{2}\left(0 \pm \sqrt{0 - \pi^2(2n+1)^2}\right) = \frac{i(2n+1)\pi}{2}, \quad n \in \mathbb{Z} \tag{2.18}$$

and

$$\begin{pmatrix} i_n(x) \\ v_n(x) \end{pmatrix} = \begin{pmatrix} \cosh\left(\frac{i(2n+1)\pi}{2}x\right) \\ \sinh\left(\frac{i(2n+1)\pi}{2}x\right) \end{pmatrix} = \begin{pmatrix} \cos\left(\frac{(2n+1)\pi}{2}x\right) \\ i \sin\left(\frac{(2n+1)\pi}{2}x\right) \end{pmatrix}. \tag{2.19}$$

Having derived the expression for the eigenvalues of $\mathcal{A}_k(P_0)$, for $k = 1, 2$, in the next chapter the expression for the eigenvalues of a perturbation of P_0 will refined to $O(1/n^2)$.

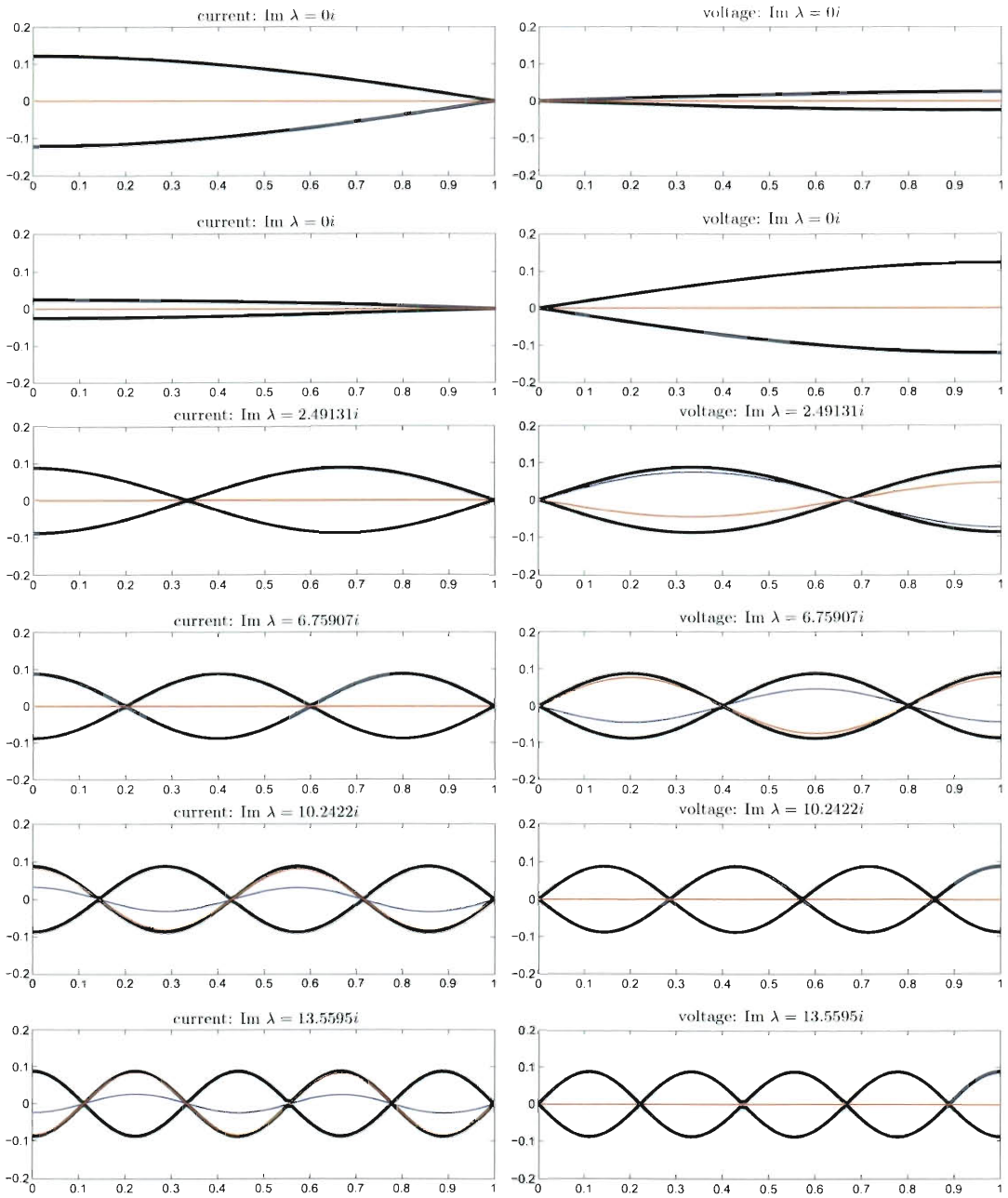

Figure 2.4 : The first few eigenvectors of $\mathcal{A}_2(P_0)$ for $g_0 = 2$ and $r_0 = 10$. The blue curve is the real part of the eigenfunction, and the red curve is the imaginary part of the eigenfunction. The black curves are the positive and negative absolute value of the eigenfunction.

Chapter 3

Refining the Asymptotic Expression for the Eigenvalues of $\mathcal{A}_1(P)$

The eigenvalue problem for (1.3) with boundary conditions $v(0) = v(1) = 0$ can be written as: find $u \neq 0, u \in D_1$ such that

$$\mathcal{A}_1(P)u = \lambda u. \tag{3.1}$$

Cox and Knobel [4] derive the following expression for the eigenvalues of $\mathcal{A}_1(P)$:

$$\lambda_n(P) = \frac{1}{2}\int_0^1 \text{tr } P(x)dx + in\pi + O(1/|n|). \tag{3.2}$$

They also derive the following expression for the eigenvector, $u(x, \lambda_n(P))$, corresponding to $\lambda_n(P)$, [4]

$$u(x, \lambda_n(P)) = \begin{pmatrix} \cosh\left(\frac{x}{2}\int_0^1 \text{tr } P(s)ds - \frac{1}{2}\int_0^x \text{tr } P(s)ds + in\pi x\right) \\ \sinh\left(\frac{x}{2}\int_0^1 \text{tr } P(s)ds - \frac{1}{2}\int_0^x \text{tr } P(s)ds + in\pi x\right) \end{pmatrix} + O(1/|n|). \tag{3.3}$$

Also given is the expression for the eigenvector, $w(x, \overline{\lambda_n}(P))$, corresponding to the eigenvalue $\overline{\lambda_n}(P)$ of the adjoint $\mathcal{A}_1^*(P)$,

$$w(x, \overline{\lambda_n}(P)) = \begin{pmatrix} \cosh\left(\frac{x}{2}\int_0^1 \text{tr } P(s)ds - \frac{1}{2}\int_0^x \text{tr } P(s)ds - in\pi x\right) \\ -\sinh\left(\frac{x}{2}\int_0^1 \text{tr } P(s)ds - \frac{1}{2}\int_0^x \text{tr } P(s)ds - in\pi x\right) \end{pmatrix} + O(1/|n|), \tag{3.4}$$

where $\mathcal{A}_1^*(P) \equiv -B\partial_x + P$ [4].

3.1 Refining the Asymptotic Expression for the "Shooting Function"

The goal of this research is to refine the asymptotic expression in (3.2) to $O(1/n^2)$. To accomplish this goal, first the expression for the"shooting function" must be refined to $O(1/n^2)$. Finding this expression for the "shooting function" requires two solutions to an equation very similar to (3.1), involving a "fake potential," be found, arguing as in the papers by Cox and Zuazua and Cox and Embree [5, 3]. These two solutions will be combined using variation of parameters to obtain a Volterra integral equation of the second kind. Then, an expression for a solution of (3.1) can be written in Neumann series form. This will result in an expression for the "shooting function" that will be used in the next section to improve the accuracy of the expression for $\lambda_n(P)$.

The equation

$$\mathcal{A}_1(P)y = B\partial_x y + P(x)y = \lambda y, \quad y(0,\lambda) = (1,0)^T \tag{3.5}$$

cannot be directly solved for y when r and g are not constant. To begin working to refine the expression for the "shooting function," I will try to find an equation very similar to (3.5) that can be (easily) solved. Let

$$f(x,\lambda) \equiv \lambda x - \frac{1}{2}\int_0^x [r(s)+g(s)]\,ds = \lambda x - \frac{1}{2}\int_0^x \text{ tr } P(s)ds. \tag{3.6}$$

If

$$z(x,\lambda) \equiv \begin{pmatrix} \cosh f(x,\lambda) \\ \sinh f(x,\lambda) \end{pmatrix}, \tag{3.7}$$

then

$$B\partial_x z(x,\lambda) + P(x)z(x,\lambda) + F(x)z(x,\lambda) = \lambda z(x,\lambda), \tag{3.8}$$

where

$$F(x) = \frac{g(x) - r(x)}{2} \begin{pmatrix} 1 & 0 \\ 0 & -1 \end{pmatrix}. \tag{3.9}$$

The computation to verify that (3.7) solves (3.8) is included in the appendix.

Now, (3.8) is almost the same as (3.5), except for the term involving F. This F is called the "fake potential."

To use variation of parameters, a second solution of (3.8), $\hat{z}(x, \lambda)$, is needed, where $z(x, \lambda)$ and $\hat{z}(x, \lambda)$ are linearly independent. One possibility for $\hat{z}(x, \lambda)$ is

$$\hat{z}(x, \lambda) \equiv Bz(x, \lambda) = \begin{pmatrix} \sinh f(x, \lambda) \\ \cosh f(x, \lambda) \end{pmatrix}. \tag{3.10}$$

The computation to verify that (3.10) is another solution of (3.8) is also included in the appendix.

Let Φ be the 2×2 matrix made by the column vectors $z(x, \lambda)$ and $\hat{z}(x, \lambda)$,

$$\Phi(x, \lambda) = \begin{pmatrix} \cosh f(x, \lambda) & \sinh f(x, \lambda) \\ \sinh f(x, \lambda) & \cosh f(x, \lambda) \end{pmatrix}.$$

Since $\det \Phi(x) = \cosh^2(f(x, \lambda)) - \sinh^2(f(x, \lambda)) = 1$, it is verified that $z(x, \lambda)$ and $\hat{z}(x, \lambda)$ are linearly independent. With these two linearly independent solutions of (3.8), variation of parameters can be used to find a solution of

$$B\partial_x y + P(x)y + F(x)y = \lambda y + F(x)y, \tag{3.11}$$

which is equivalent to (3.5).

The $y(x,\lambda)$ that solves (3.11) also solves

$$
\begin{aligned}
y(x,\lambda) &= \Phi(x,\lambda)\left[\int_0^x \Phi^{-1}(s,\lambda)BF(s)y(s,\lambda)ds + \begin{pmatrix} 1 \\ 0 \end{pmatrix}\right] \\
&= \Phi(x,\lambda)\int_0^x \frac{g(x)-r(x)}{2}\begin{pmatrix} \cosh f(s,\lambda) & -\sinh f(s,\lambda) \\ -\sinh f(s,\lambda) & \cosh f(s,\lambda) \end{pmatrix}\begin{pmatrix} 1 & 0 \\ 0 & -1 \end{pmatrix} y(s,\lambda)ds \\
&\qquad + \begin{pmatrix} \cosh f(x,\lambda) \\ \sinh f(x,\lambda) \end{pmatrix} \\
&= z(x,\lambda) + \Phi(x,\lambda)\int_0^x \frac{g(x)-r(x)}{2}\begin{pmatrix} -\sinh f(s,\lambda) & -\cosh f(s,\lambda) \\ \cosh f(s,\lambda) & \sinh f(s,\lambda) \end{pmatrix} y(s,\lambda)ds,
\end{aligned}
\tag{3.12}
$$

which is a Volterra integral equation of the second kind, arrived at by arguing as in Redheffer and Port [13, p. 354]. The computation to verify that (3.12) solves (3.11) is included in the appendix.

The y that solves the Volterra integral equation in (3.12) can be written in Neumann series form by

$$y(x,\lambda) = z(x,\lambda) + \sum_{n=1}^{\infty} S_n(x,\lambda), \tag{3.13}$$

where $S_0(x,\lambda) = z(x,\lambda)$ and

$$
\begin{aligned}
S_n(x,\lambda) &= \Phi(x,\lambda)\int_0^x \Phi^{-1}(s,\lambda)BF(s)S_{n-1}(s,\lambda)ds \\
&= \Phi(x,\lambda)\int_0^x \frac{g(s)-r(s)}{2}\begin{pmatrix} -\sinh f(s,\lambda) & -\cosh f(s,\lambda) \\ \cosh f(s,\lambda) & \sinh f(s,\lambda) \end{pmatrix} S_{n-1}(s,\lambda)ds,
\end{aligned}
\tag{3.14}
$$

as in [12, 5]. In order to extend the expression for y to $O(1/\lambda^2)$, only $S_1(x,\lambda)$ must

be computed. We have

$$S_1(x,\lambda) = \Phi(x,\lambda)\int_0^x \Phi^{-1}(s,\lambda)BF(s)z(s,\lambda)ds$$

$$= \Phi(x,\lambda)\int_0^x \frac{r(s)-g(s)}{2}\begin{pmatrix} \sinh f(s,\lambda) & \cosh f(s,\lambda) \\ -\cosh f(s,\lambda) & -\sinh f(s,\lambda)\end{pmatrix}\begin{pmatrix}\cosh f(s) \\ \sinh f(s)\end{pmatrix} ds$$

$$= \Phi(x,\lambda)\int_0^x \frac{r(s)-g(s)}{2}\begin{pmatrix} \cosh f(s,\lambda)\sinh f(s,\lambda)+\cosh f(s,\lambda)\sinh f(s,\lambda) \\ -\cosh^2 f(s,\lambda)-\sinh^2 f(s,\lambda)\end{pmatrix} ds$$

$$= \Phi(x,\lambda)\int_0^x \frac{1}{2}\begin{pmatrix} (r(s)-g(s))\sinh(2f(s,\lambda)) \\ (g(s)-r(s))\cosh(2f(s,\lambda))\end{pmatrix} ds. \quad (3.15)$$

In order to integrate (3.15) more easily, some preliminary work is helpful. For now, $b(x)$ will be a general function of x to stand in the place of linear combinations of $r(x)$ and $g(x)$, and let

$$d(x) = \int_0^x [r(t)+g(t)]dt. \quad (3.16)$$

To start, using integration by parts,

$$\int_0^x b(t)e^{\pm 2f(t,\lambda)}dt = \int_0^x b(t)e^{\pm 2\lambda t}e^{\mp d(t)}dt =$$

$$= \frac{\pm e^{\pm 2\lambda t}}{2\lambda}b(t)e^{\mp d(t)}\Big|_0^x - \int_0^x \frac{\pm e^{\pm 2\lambda t}}{2\lambda}\big(b'(t)\mp b(t)[r(t)+g(t)]\big)e^{\mp d(t)}dt$$

$$= \pm\frac{b(x)}{2\lambda}e^{\pm 2f(x,\lambda)} \mp \frac{b(0)}{2\lambda} \mp \frac{1}{2\lambda}\int_0^x \big(b'(t)\mp b(t)[r(t)+g(t)]\big)e^{\pm 2f(t,\lambda)}dt. \quad (3.17)$$

Therefore,

$$\begin{aligned}
\int_0^x b(t)\cosh(2f(t,\lambda))dt &= \frac{1}{2}\int_0^x b(t)\left(e^{2f(t,\lambda)}+e^{-2f(t,\lambda)}\right)dt = \\
&= \frac{1}{2}\left[\frac{b(x)}{2\lambda}e^{2f(x,\lambda)} - \frac{b(0)}{2\lambda} - \frac{1}{2\lambda}\int_0^x \big(b'(t)-b(t)[r(t)+g(t)]\big)e^{2f(t,\lambda)}dt\right. \\
&\quad \left. + \frac{b(0)}{2\lambda} - \frac{b(x)}{2\lambda}e^{-2f(x,\lambda)} + \frac{1}{2\lambda}\int_0^x \big(b'(t)+b(t)[r(t)+g(t)]\big)e^{-2f(t,\lambda)}dt\right] \\
&= \frac{1}{2}\left[\frac{b(x)}{2\lambda}\left(e^{2f(x,\lambda)}-e^{-2f(x,\lambda)}\right) - \frac{1}{2\lambda}\int_0^x \big(b'(t)-b(t)[r(t)+g(t)]\big)e^{2f(t,\lambda)}dt\right. \\
&\quad \left. + \frac{1}{2\lambda}\int_0^x \big(b'(t)+b(t)[r(t)+g(t)]\big)e^{-2f(t,\lambda)}dt\right] \\
&= \frac{b(x)}{2\lambda}\sinh(2f(x,\lambda)) - \frac{1}{4\lambda}\int_0^x b'(t)\left(e^{2f(t,\lambda)}-e^{-2f(t,\lambda)}\right)dt \\
&\quad + \frac{1}{4\lambda}\int_0^x 2b(t)[r(t)+g(t)]\left(e^{2f(t,\lambda)}+e^{-2f(t,\lambda)}\right)dt \\
&= \frac{b(x)}{2\lambda}\sinh(2f(x,\lambda)) - \frac{1}{2\lambda}\int_0^x b'(t)\sinh(2(f(t,\lambda))dt \\
&\quad + \frac{1}{\lambda}\int_0^x b(t)[r(t)+g(t)]\cosh(2f(t,\lambda))dt \qquad (3.18)
\end{aligned}$$

and

$$\begin{aligned}
\int_0^x b(t)\sinh(2f(t,\lambda))dt &= \frac{1}{2}\int_0^x b(t)\left(e^{2f(t,\lambda)}-e^{-2f(t,\lambda)}\right)dt \\
&= \frac{1}{2}\left[\frac{b(x)}{2\lambda}e^{2f(x,\lambda)} - \frac{b(0)}{2\lambda} - \frac{1}{2\lambda}\int_0^x \big(b'(t)-b(t)[r(t)+g(t)]\big)e^{2f(t,\lambda)}dt\right. \\
&\quad \left. - \frac{b(0)}{2\lambda} + \frac{b(x)}{2\lambda}e^{-2f(x,\lambda)} - \frac{1}{2\lambda}\int_0^x \big(b'(t)+b(t)[r(t)+g(t)]\big)e^{-2f(t,\lambda)}dt\right] \\
&= \frac{1}{2}\left[\frac{b(x)}{2\lambda}\left(e^{2f(x,\lambda)}+e^{-2f(x,\lambda)}\right) - \frac{b(0)}{\lambda} - \frac{1}{2\lambda}\int_0^x b'(t)\left(e^{2f(t,\lambda)}+e^{-2f(t,\lambda)}\right)dt\right. \\
&\quad \left. + \frac{1}{2\lambda}\int_0^x b(t)[r(t)+g(t)]\left(e^{2f(t,\lambda)}-e^{-2f(t,\lambda)}\right)dt\right] \\
&= \frac{b(x)}{2\lambda}\cosh(2f(x,\lambda)) - \frac{b(0)}{2\lambda} - \frac{1}{2\lambda}\int_0^x b'(t)\cosh(2f(t,\lambda))dt \\
&\quad + \frac{1}{\lambda}\int_0^x b(t)[r(t)+g(t)]\sinh(2f(t,\lambda))dt. \qquad (3.19)
\end{aligned}$$

Therefore, the integral expression in the top line of (3.15) becomes

$$\int_0^x \frac{1}{2}[r(s)-g(s)]\sinh(2f(s,\lambda))ds$$
$$= \frac{1}{2}\left[\frac{r(x)-g(x)}{2\lambda}\cosh(2f(x,\lambda)) - \frac{r(0)-g(0)}{2\lambda} + O(1/\lambda^2)\right], \quad (3.20)$$

and the integral expression in the bottom line of (3.15) becomes

$$\int_0^x \frac{1}{2}[g(s)-r(s)]\cosh(2f(s,\lambda))ds = \frac{1}{2}\left[\frac{g(x)-r(x)}{2\lambda}\sinh(2f(x,\lambda)) + O(1/\lambda^2)\right]. \quad (3.21)$$

Hence,

$$S_1(x,\lambda) = \Phi(x,\lambda)\int_0^x \frac{1}{2}\begin{pmatrix} (r(s)-g(s))\sinh(2f(s,\lambda)) \\ (g(s)-r(s))\cosh(2f(s,\lambda)) \end{pmatrix} ds$$

$$= \frac{1}{2}\begin{pmatrix} \cosh f(x,\lambda) & \sinh f(x,\lambda) \\ \sinh f(x,\lambda) & \cosh f(x,\lambda) \end{pmatrix}\begin{pmatrix} \frac{g(0)-r(0)}{2\lambda} + \frac{r(x)-g(x)}{2\lambda}\cosh(2f(x,\lambda)) + O(1/\lambda^2) \\ \frac{g(x)-r(x)}{2\lambda}\sinh(2f(x,\lambda)) + O(1/\lambda^2) \end{pmatrix}$$

$$= \frac{1}{2}\begin{pmatrix} \frac{r(x)-g(x)}{2\lambda}[\cosh(2f(x,\lambda))\cosh f(x,\lambda) - \sinh(2f(x,\lambda))\sinh f(x,\lambda)] \\ \frac{r(x)-g(x)}{2\lambda}[\cosh(2f(x,\lambda))\sinh f(x,\lambda) - \sinh(2f(x,\lambda))\cosh f(x,\lambda)] \end{pmatrix}$$
$$+ \frac{1}{2}\begin{pmatrix} \frac{g(0)-r(0)}{2\lambda}\cosh f(x,\lambda) \\ \frac{g(0)-r(0)}{2\lambda}\sinh f(x,\lambda) \end{pmatrix} + O(1/\lambda^2)$$

$$= \frac{1}{4\lambda}\begin{pmatrix} (g(0)-r(0))\cosh f(x,\lambda) + [r(x)-g(x)]\cosh f(x,\lambda) \\ (g(0)-r(0))\sinh f(x,\lambda) - [r(x)-g(x)]\sinh f(x,\lambda) \end{pmatrix} + O(1/\lambda^2)$$

$$= \frac{1}{4\lambda}\begin{pmatrix} (g(0)-r(0)+r(x)-g(x))\cosh f(x,\lambda) \\ (g(0)-r(0)-r(x)+g(x))\sinh f(x,\lambda) \end{pmatrix} + O(1/\lambda^2). \quad (3.22)$$

Now the components of y can be written

$$u_1(x,\lambda) = \cosh f(x,\lambda) + \frac{g(0)-r(0)+r(x)-g(x)}{4\lambda}\cosh f(x,\lambda) + O(1/\lambda^2) \quad (3.23)$$

$$u_2(x,\lambda) = \sinh f(x,\lambda) + \frac{g(0)-r(0)-r(x)+g(x)}{4\lambda}\sinh f(x,\lambda) + O(1/\lambda^2). \quad (3.24)$$

The eigenvalues of $\mathcal{A}_1(P)$ are the $\lambda_n(P)$ such that $y_2(1, \lambda_n(P)) = 0$ and the eigenvectors are $u(x, \lambda_n(P)) \equiv y(x, \lambda_n(P))$.

3.2 Refining the Asymptotic Expression for $\lambda_n(P)$

In their paper, Cox and Embree [3] refined the expressions for the eigenvalues and eigenvectors of the damped wave operator of $O(1/|n|)$ from Cox and Zuazua [5] and arrived at expressions of $O(1/n^2)$. In this section, the expressions for the eigenvalues and eigenvectors of the operator from the telegrapher's equation of $O(1/|n|)$ from Cox and Knobel [4] are put through a similar procedure to arrive at expressions of $O(1/n^2)$.

Given $P(x)$, let

$$P_0 \equiv \int_0^1 P(x)dx = \begin{pmatrix} r_0 & 0 \\ 0 & g_0 \end{pmatrix} \quad \text{and} \quad \widetilde{P}(x) \equiv P(x) - P_0 = \begin{pmatrix} \widetilde{r}(x) & 0 \\ 0 & \widetilde{g}(x) \end{pmatrix}.$$

Equation (3.2) can now be written as

$$\lambda_n(P) = \frac{1}{2}\text{tr } P_0 + in\pi + O(1/|n|). \tag{3.25}$$

This expression was shown by Cox and Knobel to be valid for *simple* matrices, as defined in Chapter 2 [4]. The goal of this research is to specify the $O(1/|n|)$ term in the expression for λ_n in (3.25). Arguing as in Cox and Embree and Pöschel and Trubowitz, [3, 12], I will start with the identity

$$\lambda_n(P_0 + \widetilde{P}) - \lambda_n(P_0) = \int_0^1 \frac{d}{dt}\lambda_n(P_0 + t\widetilde{P})dt, \tag{3.26}$$

which is valid for *simple* P_0 and small $\widetilde{P}$.

Let

$$\hat{t} \equiv P_0 + t\widetilde{P}. \tag{3.27}$$

Then

$$u(x, \lambda_n(\hat{t})) = u(x, \lambda_n(P_0 + t\widetilde{P})),$$

$$w(x, \overline{\lambda_n}(\hat{t})) \equiv w(x, \overline{\lambda_n}(P_0 + t\widetilde{P})) = \begin{pmatrix} 1 & 0 \\ 0 & -1 \end{pmatrix} u(x, \overline{\lambda_n}(\hat{t})),$$

$$\mathcal{A}_1(\hat{t})u(x, \lambda_n(\hat{t})) = \lambda_n(\hat{t})u(x, \lambda_n(\hat{t})),$$

and

$$\mathcal{A}_1^*(\hat{t})w(x, \overline{\lambda_n}(\hat{t})) = \overline{\lambda_n}(\hat{t})w(x, \overline{\lambda_n}(\hat{t})). \tag{3.28}$$

Now the expression in (3.6) becomes

$$\begin{aligned} f(x, \lambda_n(\hat{t})) &= \lambda_n(\hat{t})x - \frac{1}{2}\int_0^x \Big(\text{tr } P_0 + t \text{ tr } \widetilde{P}(s) \Big) ds \\ &= \left[\frac{1}{2} \text{ tr } P_0 + in\pi + O(1/|n|) \right] x - \frac{1}{2}\int_0^x \text{ tr } P_0 ds - \frac{t}{2}\int_0^x \text{ tr } \widetilde{P}(s) ds \\ &= \frac{x}{2} \text{ tr } P_0 + in\pi x + O(1/|n|) - \frac{x}{2} \text{ tr } P_0 - \frac{t}{2}\int_0^x \text{ tr } \widetilde{P}(s) ds \\ &= in\pi x - \frac{t}{2}\int_0^x \text{ tr } \widetilde{P}(s) ds + O(1/|n|). \end{aligned}$$

Let

$$\xi(x) \equiv -\frac{1}{2}\int_0^x \text{ tr } \widetilde{P}(s) ds. \tag{3.29}$$

Then

$$f(x, \lambda_n(\hat{t})) = t\xi(x) + in\pi x + O(1/|n|). \tag{3.30}$$

For *simple* P_0 and small $\widetilde{P}$, an expression involving the integrand of (3.26) can be obtained after taking the derivative, with respect to t, of

$$\mathcal{A}_1(\hat{t})u(x, \lambda_n(\hat{t})) = \lambda_n(\hat{t})u(x, \lambda_n(\hat{t})), \tag{3.31}$$

as in [3]. Let $\dot{s} = ds/dt$; then the derivative with respect to t of (3.31) is

$$\dot{\mathcal{A}}_1(\hat{t})u(x, \lambda_n(\hat{t})) + \mathcal{A}_1(\hat{t})\dot{u}(x, \lambda_n(\hat{t})) = \dot{\lambda}_n(\hat{t})u(x, \lambda_n(\hat{t})) + \lambda_n(\hat{t})\dot{u}(x, \lambda_n(\hat{t})). \tag{3.32}$$

The $L^2(0,1) \times L^2(0,1)$ inner product is

$$\left\langle \begin{pmatrix} a \\ b \end{pmatrix}, \begin{pmatrix} c \\ d \end{pmatrix} \right\rangle = \int_0^1 \left(a\bar{c} + b\overline{d}\right) dx. \tag{3.33}$$

To isolate the desired term, $\dot{\lambda}_n(\hat{t})$, first take the inner product of each side of (3.32) with the associated adjoint eigenvector, $w(x, \overline{\lambda_n}(\hat{t}))$:

$$\begin{aligned} &\left\langle \dot{\mathcal{A}}_1(\hat{t})u(x,\lambda_n(\hat{t})) + \mathcal{A}_1(\hat{t})\dot{u}(x,\lambda_n(\hat{t})), w(x,\overline{\lambda_n}(\hat{t}))\right\rangle \\ &\qquad = \left\langle \dot{\lambda}_n(\hat{t})u(x,\lambda_n(\hat{t})) + \lambda_n(\hat{t})\dot{u}(x,\lambda_n(\hat{t})), w(x,\overline{\lambda_n}(\hat{t}))\right\rangle. \end{aligned} \tag{3.34}$$

Using properties of the inner product and (3.28) (and suppressing the arguments, for now), the expression in (3.34) becomes

$$\begin{aligned} &\langle \dot{\mathcal{A}}_1 u, w\rangle + \langle \mathcal{A}_1\dot{u}, w\rangle = \langle \dot{\lambda}_n u, w\rangle + \langle \lambda_n \dot{u}, w\rangle \\ &\langle \dot{\mathcal{A}}_1 u, w\rangle + \langle \dot{u}, \mathcal{A}_1^* w\rangle = \\ &\langle \dot{\mathcal{A}}_1 u, w\rangle + \langle \dot{u}, \overline{\lambda_n} w\rangle = \\ &\langle \dot{\mathcal{A}}_1 u, w\rangle + \lambda_n\langle \dot{u}, w\rangle = \dot{\lambda}_n\langle u, w\rangle + \lambda_n\langle \dot{u}, w\rangle. \end{aligned}$$

Therefore,

$$\langle \dot{\mathcal{A}}_1(\hat{t})u(x,\lambda_n(\hat{t})), w(x,\overline{\lambda_n}(\hat{t}))\rangle = \dot{\lambda}_n(\hat{t})\langle u(x,\lambda_n(\hat{t})), w(x,\overline{\lambda_n}(\hat{t}))\rangle. \tag{3.35}$$

First focusing on the right side of (3.35), the inner product is

$$\begin{aligned} \langle u(x,\lambda_n(\hat{t})), w(x,\overline{\lambda_n}(\hat{t}))\rangle &= \left\langle \begin{pmatrix} u_1(x,\lambda_n(\hat{t})) \\ u_2(x,\lambda_n(\hat{t})) \end{pmatrix}, \begin{pmatrix} u_1(x,\lambda_n(\hat{t})) \\ -u_2(x,\lambda_n(\hat{t})) \end{pmatrix} \right\rangle \\ &= \int_0^1 \left[u_1(x,\lambda_n(\hat{t}))\overline{u_1(x,\lambda_n(\hat{t}))} + u_2(x,\lambda_n(\hat{t}))\overline{(-1)u_2(x,\lambda_n(\hat{t}))}\right] dx \\ &= \int_0^1 \left[u_1^2(x,\lambda_n(\hat{t})) - u_2^2(x,\lambda_n(\hat{t}))\right] dx. \end{aligned} \tag{3.36}$$

To compute (3.36), more specific details are needed from (3.23) and (3.24). For (3.23),

$$\begin{aligned} u_1(x,\lambda_n(\hat{t})) &= u_1(x,\lambda_n(P_0+t\widetilde{P})) \\ &= \frac{g_0+t\widetilde{g}(0)-r_0-t\widetilde{r}(0)+r_0+t\widetilde{r}(x)-g_0-t\widetilde{g}(x)}{4\lambda_n(\hat{t})}\cosh f(x,\lambda_n(\hat{t})) \\ &\qquad + \cosh f(x,\lambda_n(\hat{t})) + O(1/\lambda_n^2(\hat{t})) \\ &= \left(1+\frac{t[\widetilde{g}(0)-\widetilde{r}(0)+\widetilde{r}(x)-\widetilde{g}(x)]}{4\lambda_n(\hat{t})}\right)\cosh f(x,\lambda_n(\hat{t})) + O(1/n^2). \end{aligned} \tag{3.37}$$

Then,

$$\begin{aligned} u_1^2(x,\lambda_n(\hat{t})) &= \left(1+\frac{t[\widetilde{g}(0)-\widetilde{r}(0)+\widetilde{r}(x)-\widetilde{g}(x)]}{4\lambda_n(\hat{t})}\right)^2\cosh^2 f(x,\lambda_n(\hat{t})) + O(1/n^2) \\ &= \left(\frac{t[\widetilde{g}(0)-\widetilde{r}(0)+\widetilde{r}(x)-\widetilde{g}(x)]}{2\lambda_n(\hat{t})}+\frac{t^2[\widetilde{g}(0)-\widetilde{r}(0)+\widetilde{r}(x)-\widetilde{g}(x)]^2}{16\lambda_n^2(\hat{t})}\right)\cosh^2 f(x,\lambda_n(\hat{t})) \\ &\qquad + \cosh^2 f(x,\lambda_n(\hat{t})) + O(1/n^2) \\ &= \left(1+\frac{t[\widetilde{g}(0)-\widetilde{r}(0)+\widetilde{r}(x)-\widetilde{g}(x)]}{2\lambda_n(\hat{t})}\right)\cosh^2 f(x,\lambda_n(\hat{t})) + O(1/n^2). \end{aligned} \tag{3.38}$$

For (3.24),

$$\begin{aligned} u_2(x,\lambda_n(\hat{t})) &= u_2(x,\lambda_n(P_0+t\widetilde{P})) \\ &= \frac{g_0+t\widetilde{g}(0)-r_0-t\widetilde{r}(0)-r_0-t\widetilde{r}(x)+g_0+t\widetilde{g}(x)}{4\lambda_n(\hat{t})}\sinh(f(x,\lambda_n(\hat{t}))) \\ &\qquad + \sinh f(x,\lambda_n(\hat{t})) + O(1/\lambda_n^2(\hat{t})) \\ &= \left(1+\frac{2g_0-2r_0+t[\widetilde{g}(0)-\widetilde{r}(0)-\widetilde{r}(x)+\widetilde{g}(x)]}{4\lambda_n(\hat{t})}\right)\sinh(f(x,\lambda_n(\hat{t}))) + O(1/n^2). \end{aligned} \tag{3.39}$$

Then,

$$\begin{aligned} u_2^2(x,\lambda_n(\hat{t})) &= \left(1+\frac{2g_0-2r_0+t[\widetilde{g}(0)-\widetilde{r}(0)-\widetilde{r}(x)+\widetilde{g}(x)]}{4\lambda_n(\hat{t})}\right)^2\sinh^2(f(x,\lambda_n(\hat{t}))) \\ &\qquad + O(1/n^2) \end{aligned}$$

$$u_2^2(x,\lambda_n(\hat{t})) = \left(1+\frac{2g_0-2r_0+t[\widetilde{g}(0)-\widetilde{r}(0)-\widetilde{r}(x)+\widetilde{g}(x)]}{2\lambda_n(\hat{t})} + \frac{(2g_0-2r_0+t[\widetilde{g}(0)-\widetilde{r}(0)-\widetilde{r}(x)+\widetilde{g}(x)])^2}{16\lambda_n^2(\hat{t})}\right)\sinh^2(f(x,\lambda_n(\hat{t}))) + O(1/n^2)$$
$$= \left(1+\frac{2g_0-2r_0+t[\widetilde{g}(0)-\widetilde{r}(0)-\widetilde{r}(x)+\widetilde{g}(x)]}{2\lambda_n(\hat{t})}\right)\sinh^2(f(x,\lambda_n(\hat{t}))) + O(1/n^2). \tag{3.40}$$

Now the integrand in (3.36) can be simplified as

$$\begin{aligned} u_1^2(x,\lambda_n(\hat{t})) - u_2^2(x,\lambda_n(\hat{t})) &= \cosh^2 f(x,\lambda_n(\hat{t})) - \sinh^2(f(x,\lambda_n(\hat{t}))) \\ &\quad + \frac{t[\widetilde{g}(0)-\widetilde{r}(0)+\widetilde{r}(x)-\widetilde{g}(x)]}{2\lambda_n(\hat{t})}\cosh^2 f(x,\lambda_n(\hat{t})) \\ &\quad - \frac{2g_0-2r_0+t[\widetilde{g}(0)-\widetilde{r}(0)-\widetilde{r}(x)+\widetilde{g}(x)]}{2\lambda_n(\hat{t})}\sinh^2(f(x,\lambda_n(\hat{t}))) + O(1/n^2) \\ &= 1 + O(1/|n|). \end{aligned} \tag{3.41}$$

Therefore, the inner product on the right side of (3.35) can be written as

$$\langle u(x,\lambda_n(\hat{t})), w(x,\overline{\lambda_n}(\hat{t}))\rangle = \int_0^1 [1+O(1/|n|)]\,dx = 1+O(1/|n|). \tag{3.42}$$

Now focusing on the left side of (3.35), since $\mathcal{A}_1(\hat{t}) = \mathcal{A}_1(P_0+t\widetilde{P}) = B\partial_x + P_0 + t\widetilde{P}$, $\dot{\mathcal{A}}_1(\hat{t}) = \widetilde{P}$, and the left side of (3.35) becomes

$$\begin{aligned} \langle \dot{\mathcal{A}}_1(\hat{t})u(x,\lambda_n(\hat{t})), w(x,\overline{\lambda_n}(\hat{t}))\rangle &= \langle \widetilde{P}(x)u(x,\lambda_n(\hat{t})), w(x,\overline{\lambda_n}(\hat{t}))\rangle \\ &= \left\langle \begin{pmatrix} \widetilde{r}(x)u_1(x,\lambda_n(\hat{t})) \\ \widetilde{g}(x)u_2(x,\lambda_n(\hat{t})) \end{pmatrix}, \begin{pmatrix} u_1(x,\lambda_n(\hat{t})) \\ -u_2(x,\lambda_n(\hat{t})) \end{pmatrix} \right\rangle \\ &= \int_0^1 \left[\widetilde{r}(x)u_1^2(x,\lambda_n(\hat{t})) - \widetilde{g}(x)u_2^2(x,\lambda_n(\hat{t}))\right] dx. \end{aligned} \tag{3.43}$$

Using (3.38) and (3.40), the integrand from (3.43) becomes

$$\begin{aligned}
&\widetilde{r}(x)u_1^2(x,\lambda_n(\hat{t})) - \widetilde{g}(x)u_2^2(x,\lambda_n(\hat{t})) = \\
&\qquad = \widetilde{r}(x)\left(1 + \frac{t[\widetilde{g}(0) - \widetilde{r}(0) + \widetilde{r}(x) - \widetilde{g}(x)]}{2\lambda_n(\hat{t})}\right)\cosh^2 f(x,\lambda_n(\hat{t})) \\
&- \widetilde{g}(x)\left(1 + \frac{2g_0 - 2r_0 + t[\widetilde{g}(0) - \widetilde{r}(0) - \widetilde{r}(x) + \widetilde{g}(x)]}{2\lambda_n(\hat{t})}\right)\sinh^2(f(x,\lambda_n(\hat{t}))) + O(1/n^2) \\
&\qquad = \widetilde{r}(x)\cosh^2 f(x,\lambda_n(\hat{t})) - \widetilde{g}(x)\sinh^2 f(x,\lambda_n(\hat{t})) \\
&\qquad + \frac{t[\widetilde{g}(0) - \widetilde{r}(0) + \widetilde{r}(x) - \widetilde{g}(x)]}{2\lambda_n(\hat{t})}\widetilde{r}(x)\cosh^2 f(x,\lambda_n(\hat{t})) \\
&\quad - \frac{2g_0 - 2r_0 + t[\widetilde{g}(0) - \widetilde{r}(0) - \widetilde{r}(x) + \widetilde{g}(x)]}{2\lambda_n(\hat{t})}\widetilde{g}(x)\sinh^2(f(x,\lambda_n(\hat{t}))) + O(1/n^2)
\end{aligned}$$

$$\begin{aligned}
&\widetilde{r}(x)u_1^2(x,\lambda_n(\hat{t})) - \widetilde{g}(x)u_2^2(x,\lambda_n(\hat{t})) = \\
&\qquad = \widetilde{r}(x)\cosh^2 f(x,\lambda_n(\hat{t})) - \widetilde{g}(x)\sinh^2 f(x,\lambda_n(\hat{t})) - \frac{t\widetilde{r}(x)\widetilde{g}(x)}{2\lambda_n(\hat{t})} \\
&\qquad + \frac{t[\widetilde{g}(0) - \widetilde{r}(0) + \widetilde{r}(x)]}{2\lambda_n(\hat{t})}\widetilde{r}(x)\cosh^2 f(x,\lambda_n(\hat{t})) \\
&\quad - \frac{2g_0 - 2r_0 + t[\widetilde{g}(0) - \widetilde{r}(0) + \widetilde{g}(x)]}{2\lambda_n(\hat{t})}\widetilde{g}(x)\sinh^2(f(x,\lambda_n(\hat{t}))) + O(1/n^2)
\end{aligned}$$

$$\begin{aligned}
&\widetilde{r}(x)u_1^2(x,\lambda_n(\hat{t})) - \widetilde{g}(x)u_2^2(x,\lambda_n(\hat{t})) = \widetilde{r}(x)\cosh^2 f(x,\lambda_n(\hat{t})) - \widetilde{g}(x)\sinh^2 f(x,\lambda_n(\hat{t})) \\
&\qquad + \left(\frac{t\widetilde{r}(x)[\widetilde{g}(0) - \widetilde{r}(0) + \widetilde{r}(x)]}{2\lambda_n(\hat{t})}\right)\cosh^2 f(x,\lambda_n(\hat{t})) \\
&\qquad - \left(\frac{t\widetilde{g}(x)[\widetilde{g}(0) - \widetilde{r}(0) + \widetilde{g}(x)]}{2\lambda_n(\hat{t})}\right)\sinh^2 f(x,\lambda_n(\hat{t})) \\
&\qquad - \frac{t\widetilde{r}(x)\widetilde{g}(x)}{2\lambda_n(\hat{t})} - \left(\frac{\widetilde{g}(x)[g_0 - r_0]}{\lambda_n(\hat{t})}\right)\sinh^2 f(x,\lambda_n(\hat{t})) + O(1/n^2). \quad (3.44)
\end{aligned}$$

Therefore, the inner product on the left side of (3.35) can be written as

$$\begin{aligned}
\langle \dot{\mathcal{A}}_1(\hat{t})u(x,\lambda_n(\hat{t})), w(x,\overline{\lambda_n}(\hat{t}))\rangle &= \int_0^1 \left[\widetilde{r}(x)u_1^2(x,\lambda_n(\hat{t})) - \widetilde{g}(x)u_2^2(x,\lambda_n(\hat{t}))\right] dx \\
&= J_1(\hat{t}) - J_2(\hat{t}) + J_3(\hat{t}) - J_4(\hat{t}) - J_5(\hat{t}) - J_6(\hat{t}), \quad (3.45)
\end{aligned}$$

where

$$J_1(\hat{t}) = \int_0^1 \widetilde{r}(x)\cosh^2 f(x,\lambda_n(\hat{t}))dx$$
$$J_2(\hat{t}) = \int_0^1 \widetilde{g}(x)\sinh^2 f(x,\lambda_n(\hat{t}))dx$$
$$J_3(\hat{t}) = \frac{t}{2\lambda_n(\hat{t})}\int_0^1 \widetilde{r}(x)[\widetilde{g}(0)-\widetilde{r}(0)+\widetilde{r}(x)]\cosh^2 f(x,\lambda_n(\hat{t}))dx$$
$$J_4(\hat{t}) = \frac{t}{2\lambda_n(\hat{t})}\int_0^1 \widetilde{g}(x)[\widetilde{g}(0)-\widetilde{r}(0)+\widetilde{g}(x)]\sinh^2 f(x,\lambda_n(\hat{t}))dx$$
$$J_5(\hat{t}) = \frac{t}{2\lambda_n(\hat{t})}\int_0^1 \widetilde{r}(x)\widetilde{g}(x)dx$$
$$J_6(\hat{t}) = \frac{1}{\lambda_n(\hat{t})}\int_0^1 \widetilde{g}(x)[g_0-r_0]\sinh^2 f(x,\lambda_n(\hat{t}))dx.$$

Since $\widetilde{g}(x)$ and $\widetilde{r}(x)$ are defined as the deviation of g and r, respectively, from constant,

$$\int_0^1 \widetilde{g}(x)dx = 0 \quad \text{and} \quad \int_0^1 \widetilde{r}(x)dx = 0. \tag{3.46}$$

Calculating the first piece of (3.45),

$$\begin{aligned}
J_1(\hat{t}) &= \int_0^1 \widetilde{r}(x)\cosh^2 f(x,\lambda_n(\hat{t}))dx = \int_0^1 \frac{\widetilde{r}(x)}{2}[\cosh(2f(x,\lambda_n(\hat{t}))) + 1]dx \\
&= \int_0^1 \frac{\widetilde{r}(x)}{2}dx + \int_0^1 \frac{\widetilde{r}(x)}{2}\cosh(2f(x,\lambda_n(\hat{t})))dx \\
&= 0 + \int_0^1 \frac{\widetilde{r}(x)}{2}\left[\cosh\left(2t\xi(x) + 2in\pi x + O\left(\frac{1}{|n|}\right)\right)\right]dx \\
&= \int_0^1 \frac{\widetilde{r}(x)}{2}\left[\cosh(2t\xi(x) + 2in\pi x)\cosh\left(O\left(\frac{1}{|n|}\right)\right) + \right. \\
&\qquad \left. + \sinh(2t\xi(x) + 2in\pi x)\sinh\left(O\left(\frac{1}{|n|}\right)\right)\right]dx \\
&= \int_0^1 \frac{\widetilde{r}(x)}{2}\cosh(2t\xi(x) + 2in\pi x)dx + O\left(\frac{1}{n^2}\right) \\
&= \int_0^1 \frac{\widetilde{r}(x)}{2}[\cosh(2t\xi(x))\cosh(2in\pi x) + \sinh(2t\xi(x))\sinh(2in\pi x)]dx + O\left(\frac{1}{n^2}\right) \\
&= \int_0^1 \frac{\widetilde{r}(x)}{2}[\cosh(2t\xi(x))\cos(2n\pi x) + i\sinh(2t\xi(x))\sin(2n\pi x)]dx + O\left(\frac{1}{n^2}\right).
\end{aligned} \tag{3.47}$$

Similarly,

$$\begin{aligned}
J_2(\hat{t}) &= \int_0^1 \widetilde{g}(x)\sinh^2 f(x,\lambda_n(\hat{t}))dx = \int_0^1 \frac{\widetilde{g}(x)}{2}[\cosh(2f(x,\lambda_n(\hat{t}))) - 1]dx \\
&= \int_0^1 \frac{\widetilde{g}(x)}{2}\cosh(2f(x,\lambda_n(\hat{t})))dx \\
&= \int_0^1 \frac{\widetilde{g}(x)}{2}[\cosh(2t\xi(x))\cos(2n\pi x) + i\sinh(2t\xi(x))\sin(2n\pi x)]dx + O\left(\frac{1}{n^2}\right).
\end{aligned} \tag{3.48}$$

Next,

$$\begin{aligned}
J_3(\hat{t}) &= \frac{t}{2\lambda_n(\hat{t})}\int_0^1 [\widetilde{r}(x)\widetilde{g}(0) - \widetilde{r}(x)\widetilde{r}(0) + \widetilde{r}^2(x)]\cosh^2 f(x,\lambda_n(\hat{t}))dx \\
&= \frac{t}{4\lambda_n(\hat{t})}\int_0^1 [\widetilde{r}(x)\widetilde{g}(0) - \widetilde{r}(x)\widetilde{r}(0) + \widetilde{r}^2(x)][\cosh(2f(x,\lambda_n(\hat{t}))) + 1]dx \\
&= \frac{-it}{4n\pi}\int_0^1 \widetilde{r}^2(x)dx + O\left(\frac{1}{n^2}\right).
\end{aligned} \tag{3.49}$$

Also,

$$\begin{aligned} J_4(\hat{t}) &= \frac{t}{2\lambda_n(\hat{t})}\int_0^1 [\widetilde{g}(x)\widetilde{g}(0) - \widetilde{g}(x)\widetilde{r}(0) + \widetilde{g}^2(x)]\sinh^2 f(x,\lambda_n(\hat{t}))dx \\ &= \frac{t}{4\lambda_n(\hat{t})}\int_0^1 [\widetilde{g}(x)\widetilde{g}(0) - \widetilde{g}(x)\widetilde{r}(0) + \widetilde{g}^2(x)][\cosh(2f(x,\lambda_n(\hat{t}))) - 1]dx \\ &= \frac{it}{4n\pi}\int_0^1 \widetilde{g}^2(x)dx + O\left(\frac{1}{n^2}\right) \end{aligned} \tag{3.50}$$

and

$$J_5(\hat{t}) = \frac{t}{2\lambda_n(\hat{t})}\int_0^1 \widetilde{r}(x)\widetilde{g}(x)dx = \frac{-it}{2n\pi}\int_0^1 \widetilde{r}(x)\widetilde{g}(x)dx + O\left(\frac{1}{n^2}\right). \tag{3.51}$$

Finally,

$$\begin{aligned} J_6(\hat{t}) &= \frac{1}{\lambda_n(\hat{t})}\int_0^1 \widetilde{g}(x)[g_0 - r_0]\sinh^2 f(x,\lambda_n(\hat{t}))dx \\ &= \frac{1}{2\lambda_n(\hat{t})}\int_0^1 \widetilde{g}(x)[g_0 - r_0][\cosh(2f(x,\lambda_n(\hat{t}))) - 1]dx \\ &= -\frac{1}{2\lambda_n(\hat{t})}\int_0^1 \widetilde{g}(x)[g_0 - r_0]dx + \frac{1}{2\lambda_n(\hat{t})}\int_0^1 \widetilde{g}(x)[g_0 - r_0]\cosh(2f(x,\lambda_n(\hat{t})))dx \\ &= 0 + O\left(\frac{1}{n^2}\right). \end{aligned} \tag{3.52}$$

Combining these terms, (3.45) becomes

$$\begin{aligned} &\langle \dot{\mathcal{A}}_1(\hat{t})u(x,\lambda_n(\hat{t})), w(x,\overline{\lambda_n}(\hat{t}))\rangle = \\ &\quad = \int_0^1 \frac{\widetilde{r}(x)}{2}[\cosh(2t\xi(x))\cos(2n\pi x) + i\sinh(2t\xi(x))\sin(2n\pi x)]dx + \\ &\quad - \int_0^1 \frac{\widetilde{g}(x)}{2}[\cosh(2t\xi(x))\cos(2n\pi x) + i\sinh(2t\xi(x))\sin(2n\pi x)]dx + \\ &\qquad - \frac{it}{4n\pi}\int_0^1 \widetilde{r}^2(x)dx - \frac{it}{4n\pi}\int_0^1 \widetilde{g}^2(x)dx + \frac{it}{2n\pi}\int_0^1 \widetilde{r}(x)\widetilde{g}(x)dx + O\left(\frac{1}{n^2}\right) \end{aligned}$$

$$\begin{aligned} &\langle \dot{\mathcal{A}}_1(\hat{t})u(x,\lambda_n(\hat{t})), w(x,\overline{\lambda_n}(\hat{t}))\rangle = -\frac{it}{4n\pi}\int_0^1 [\widetilde{r}(x) - \widetilde{g}(x)]^2 dx \\ &+ \int_0^1 \frac{\widetilde{r}(x) - \widetilde{g}(x)}{2}[\cosh(2t\xi(x))\cos(2n\pi x) + i\sinh(2t\xi(x))\sin(2n\pi x)]dx + O\left(\frac{1}{n^2}\right). \end{aligned} \tag{3.53}$$

With the expressions (3.42) and (3.53), for the inner product on the right and left, respectively, of (3.35), $\dot{\lambda}_n(\hat{t})$ can be written in a form that allows $\int_0^1 \dot{\lambda}_n(P_0 + t\widetilde{P})dt$ to be computed. First rewriting (3.35) and then substituting the expressions from (3.42) and (3.53),

$$\begin{aligned}
\int_0^1 \dot{\lambda}_n(P_0 + t\widetilde{P})dt = \int_0^1 \dot{\lambda}_n(\hat{t})dt &= \int_0^1 \frac{\langle \dot{\mathcal{A}}_1(\hat{t})u(x,\lambda_n(\hat{t})), w(x,\overline{\lambda_n}(\hat{t}))\rangle}{\langle u(x,\lambda_n(\hat{t})), w(x,\overline{\lambda_n}(\hat{t}))\rangle}dt \\
&= \int_0^1 \frac{J_1(\hat{t}) - J_2(\hat{t}) + J_3(\hat{t}) - J_4(\hat{t}) - J_5(\hat{t}) - J_6(\hat{t})}{1 + O(1/|n|)}dt \\
&= \int_0^1 \left\{ \int_0^1 \frac{\widetilde{r}(x) - \widetilde{g}(x)}{2} \cosh(2t\xi(x)) \cos(2n\pi x)dx \right. \\
&\quad + i\int_0^1 \frac{\widetilde{r}(x) - \widetilde{g}(x)}{2} \sinh(2t\xi(x)) \sin(2n\pi x)]dx \\
&\quad \left. - \frac{it}{4n\pi}\int_0^1 [\widetilde{r}(x) - \widetilde{g}(x)]^2 dx + O\left(\frac{1}{n^2}\right) \right\} dt.
\end{aligned}$$

Simplifying and evaluating the expression leads to

$$\begin{aligned}
\int_0^1 \dot{\lambda}_n(P_0 + t\widetilde{P})dt &= \int_0^1 \left(\frac{\widetilde{r}(x) - \widetilde{g}(x)}{2}\right) \frac{\sinh(2t\xi(x))}{2\xi(x)} \cos(2n\pi x)dx\Big|_{t=0}^{t=1} \\
&\quad + i\int_0^1 \left(\frac{\widetilde{r}(x) - \widetilde{g}(x)}{2}\right) \frac{\cosh(2t\xi(x))}{2\xi(x)} \sin(2n\pi x)dx\Big|_{t=0}^{t=1} \\
&\quad - \frac{it^2}{8n\pi}\int_0^1 [\widetilde{r}(x) - \widetilde{g}(x)]^2 dx\Big|_{t=0}^{t=1} + O\left(\frac{1}{n^2}\right) \\
&= \int_0^1 \frac{\sinh(2\xi(x))}{4\xi(x)} [\widetilde{r}(x) - \widetilde{g}(x)] \cos(2n\pi x)dx \\
&\quad + i\int_0^1 \frac{\cosh(2\xi(x)) - 1}{4\xi(x)} [\widetilde{r}(x) - \widetilde{g}(x)] \sin(2n\pi x)dx \\
&\quad - \frac{i}{8n\pi}\int_0^1 [\widetilde{r}(x) - \widetilde{g}(x)]^2 dx + O\left(\frac{1}{n^2}\right). \quad (3.54)
\end{aligned}$$

It is now possible to refine the asymptotic expression for $\lambda_n(P)$ to $O(1/n^2)$. Re-

turning to (3.26), and using (2.7) and (3.54),

$$\begin{aligned}\lambda_n(P) = \lambda_n(P_0 + \widetilde{P}) &= \lambda_n(P_0) + \int_0^1 \frac{d}{dt}\lambda_n(P_0 + t\widetilde{P})dt \\ &= \frac{r_0 + g_0}{2} + \int_0^1 \frac{\sinh(2\xi(x))}{4\xi(x)}[\widetilde{r}(x) - \widetilde{g}(x)]\cos(2n\pi x)dx \\ &\quad + i\left(n\pi - \frac{(r_0 - g_0)^2}{8n\pi}\right) - \frac{i}{8n\pi}\int_0^1 [\widetilde{r}(x) - \widetilde{g}(x)]^2 dx \\ &\quad + i\int_0^1 \frac{\cosh(2\xi(x)) - 1}{4\xi(x)}[\widetilde{r}(x) - \widetilde{g}(x)]\sin(2n\pi x)dx + O\left(\frac{1}{n^2}\right)\end{aligned}$$

$$\begin{aligned}\lambda_n(P) = \frac{r_0 + g_0}{2} &+ \int_0^1 \frac{\sinh(2\xi(x))}{4\xi(x)}[\widetilde{r}(x) - \widetilde{g}(x)]\cos(2n\pi x)dx \\ &+ in\pi - \frac{i}{8n\pi}\int_0^1 [r(x) - g(x)]^2 dx \\ &+ i\int_0^1 \frac{\cosh(2\xi(x)) - 1}{4\xi(x)}[\widetilde{r}(x) - \widetilde{g}(x)]\sin(2n\pi x)dx + O\left(\frac{1}{n^2}\right). \quad (3.55)\end{aligned}$$

This is the refined asymptotic expression for $\lambda_n(P)$ to $O(1/n^2)$.

3.3 Verifying the Accuracy of the Expression for $\lambda_n(P)$

To verify the accuracy of this expression, the eigenvalues computed from (3.55) are compared to the eigenvalues computed using the spectral discretization. (The spectral method used to calculate these eigenvalues, and some other eigenvalues presented in this thesis, is described in Chapter 7.) To generate the data in Table 3.1, $r(x) = 1+x^2$ and $g(x) = x^2$ were used. The second column of the table shows the value for λ_n calculated with spectral discretization (using $N = 128$). For this r, g, and N, we believe the eigenvalues from the spectral method are exact to the digits listed. The third column of the table shows the values for λ_n calculated with the asymptotic expression in (3.55). (For asymptotic calculations, symbolic integration and evaluation were done with Mathematica.)

Table 3.1 : Eigenvalues of $\mathcal{A}_1(P)$ when $r(x) = 1 + x^2$ and $g(x) = x^2$ calculated with spectral discretization, using $N = 128$, and with the asymptotic expression in (3.55). The underlined digits are exactly the same from spectral and asymptotic results.

n	spectral eigenvalue	asymptotic eigenvalue
1	0.8333333 + 3.1018039i	0.8294455 + 3.0936938i
2	0.8333333 + 6.2632909i	0.8330371 + 6.2623433i
3	0.8333333 + 9.4115150i	0.8332727 + 9.4112280i
4	0.8333333 + 12.5564234i	0.8333138 + 12.5563010i
5	0.8333333 + 15.7000055i	0.8333252 + 15.6999425i
6	0.8333333 + 18.8429244i	0.8333294 + 18.8428879i
7	0.8333333 + 21.9854644i	0.8333312 + 21.9854414i
8	0.8333333 + 25.1277676i	0.8333320 + 25.1277521i
9	0.8333333 + 28.2699129i	0.8333325 + 28.2699020i
10	0.8333333 + 31.4119476i	0.8333328 + 31.4119397i

In the table, the underlined digits are exactly the same from spectral results and asymptotic results. As n increases, the spectral results and asymptotic results tend to agree to more digits, since the asymptotic expression is most accurate for large n. This can be seen in Figure 3.1, for $r(x) = 1 + x^2$ and $g(x) = x^2$, where the magnitude of the difference between the value computed with the spectral code and the asymptotic expression is plotted as n increases. The line in Figure 3.1 shows a rate of decrease of $1/n^2$. Since the dots are decreasing faster than this rate, it can be concluded that the asymptotic expression is actually more accurate than $O(1/n^2)$ in this example.

The main results in this chapter is (3.55), the asymptotic expression for the eigen-

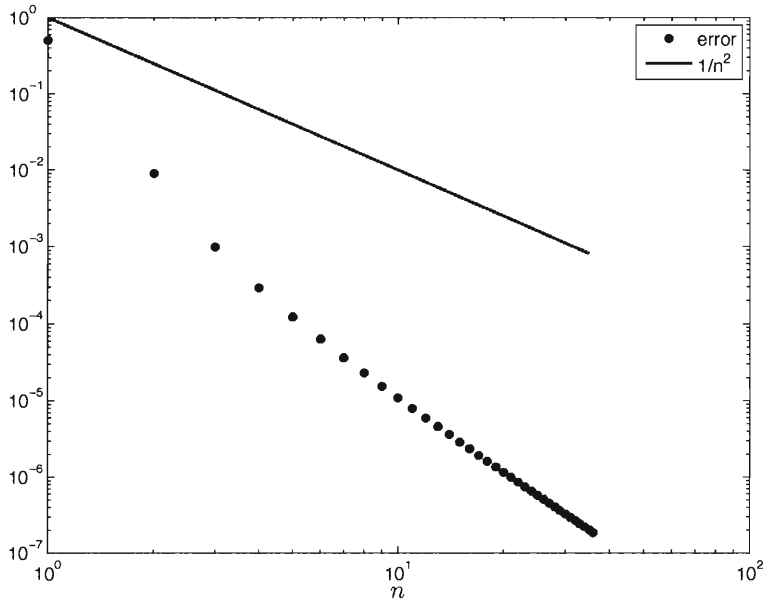

Figure 3.1 : This plot shows the decrease in the magnitude of the difference between λ_n of $\mathcal{A}_1(P)$ calculated with spectral discretization (using $N = 128$) and calculated with the asymptotic expression in (3.55) as n increases when $r(x) = 1 + x^2$ and $g(x) = x^2$.

values of $\mathcal{A}_1(P)$ to $O(1/n^2)$. This expression will be used in Chapter 5 to arrive at an expression that can be used to recover information about resistance in the telegrapher's equation.

In the next chapter, the asymptotic expression for the eigenvalues of $\mathcal{A}_2(P)$ will be refined to $O(1/n^2)$.

Chapter 4

Refining the Asymptotic Expression for the Eigenvalues of $\mathcal{A}_2(P)$

Refining the asymptotic expression for the eigenvalues of $\mathcal{A}_2(P)$ to $O(1/n^2)$ is almost exactly the same as the process of refining the asymptotic expression for the eigenvalues of $\mathcal{A}_1(P)$ that was shown in Chapter 3. The result will be presented here, noting any differences from the process in the previous chapter, omitting the details that are exactly the same.

4.1 Refining the Asymptotic Expression for $\mu_n(P)$

As in Section 3.1, the eigenvalue problem for (1.3) with boundary conditions $v(0) = i(1) = 0$ can be written as: find $\nu \neq 0, \nu \in D_2$ such that

$$\mathcal{A}_2(P)\nu = \mu\nu. \tag{4.1}$$

As Cox and Knobel state, deriving the expression for the eigenvalues of $\mathcal{A}_2(P)$ to $O(1/|n|)$ is done exactly as the derivation of the eigenvalues of $\mathcal{A}_1(P)$ to $O(1/|n|)$ [4]. The expression for $\mu_n(P)$ that parallels their result for $\lambda_n(P)$ is

$$\mu_n(P) = \frac{1}{2}\text{tr } P_0 + \frac{i(2n+1)\pi}{2} + O(1/|n|). \tag{4.2}$$

Similarly, the eigenvector, $\nu(x, \mu_n(P))$, corresponding to $\mu_n(P)$ is

$$\nu(x, \mu_n(P)) = \begin{pmatrix} \cosh\left(\xi(x) + \frac{i(2n+1)\pi x}{2}\right) \\ \sinh\left(\xi(x) + \frac{i(2n+1)\pi x}{2}\right) \end{pmatrix} + O(1/|n|), \tag{4.3}$$

and the eigenvector, $q(x, \overline{\mu_n}(P))$, corresponding to $\overline{\mu_n}(P)$, the eigenvalue of the adjoint $\mathcal{A}_2^*(P) \equiv -B\partial_x + P$, is

$$q(x, \overline{\mu_n}(P)) = \begin{pmatrix} \cosh\left(\xi(x) - \frac{i(2n+1)\pi x}{2}\right) \\ -\sinh\left(\xi(x) - \frac{i(2n+1)\pi x}{2}\right) \end{pmatrix} + O(1/|n|). \tag{4.4}$$

The equation in (4.1) cannot be solved in closed form for non-constant r and g, but using $f(x, \mu)$, from (3.6), and $z(x, \mu)$, from (3.7), leads to the same "fake potential," $F(x)$, in (3.9). Therefore, the analysis for $\mathcal{A}_2(P)$ proceeds exactly as the analysis for $\mathcal{A}_1(P)$ because the "shooting function" being used has the same initial condition of $v(0) = 0$. Variation of parameters leads to the same Volterra integral equation as before, and the solution of that integral equation can be written in the same Neumann series as before.

Therefore, the refined expression for the "shooting function" of $\mathcal{A}_2(P)$ is

$$y(x, \mu) = \begin{pmatrix} \cosh f(x, \mu) + \frac{g(0)-r(0)+r(x)-g(x)}{4\mu} \cosh f(x, \mu) \\ \sinh f(x, \mu) + \frac{g(0)-r(0)-r(x)+g(x)}{4\mu} \sinh f(x, \mu) \end{pmatrix} + O(1/\mu^2). \tag{4.5}$$

The eigenvalues of $\mathcal{A}_2(P)$ are the $\mu_n(P)$ such that $y_1(1, \mu_n(P)) = 0$ and the eigenvectors are $\nu(x, \mu_n(P)) \equiv y(x, \mu_n(P))$.

Using the same idea as in Section 3.2, the starting point to refine the expression of $\mu_n(P)$ is the identity

$$\mu_n(P_0 + \widetilde{P}) - \mu_n(P_0) = \int_0^1 \frac{d}{dt} \mu_n(P_0 + t\widetilde{P}) dt, \tag{4.6}$$

which is valid for *simple* P_0 and small $\widetilde{P}$.

Now, from (3.6),

$$\begin{aligned} f(x, \mu_n(\hat{t})) &= \mu_n(\hat{t})x - \frac{1}{2}\int_0^x \Big(\text{tr } P_0 + t \text{ tr } \widetilde{P}(s) \Big) ds \\ &= t\xi(x) + \frac{i(2n+1)\pi x}{2} + O(1/|n|), \end{aligned}$$

with ξ the same as in (3.29).

For *simple* P_0 and small $\widetilde{P}$,

$$\mathcal{A}_2(\hat{t})\nu(x,\mu_n(\hat{t})) = \mu_n(\hat{t})\nu(x,\mu_n(\hat{t})). \tag{4.7}$$

Taking the derivative with respect to t, taking the inner product of each side with the associated adjoint eigenvector, and simplifying results in

$$\langle \dot{\mathcal{A}}_2(\hat{t})\nu(x,\mu_n(\hat{t})), q(x,\overline{\mu_n}(\hat{t}))\rangle = \dot{\mu}_n(\hat{t})\langle \nu(x,\lambda_n(\hat{t})), q(x,\overline{\mu_n}(\hat{t}))\rangle. \tag{4.8}$$

By the exact same argument as in the previous chapter, the inner product on the right side of (4.8) can be written as

$$\langle \nu(x,\mu_n(\hat{t})), q(x,\overline{\mu_n}(\hat{t}))\rangle = \int_0^1 [1+O(1/|n|)]\,dx = 1+O(1/|n|). \tag{4.9}$$

The inner product on the left side of (4.8), again, after the same computations as in the previous chapter, becomes

$$\begin{aligned}\langle \dot{\mathcal{A}}_2(\hat{t})\nu(x,\mu_n(\hat{t})), q(x,\overline{\mu_n}(\hat{t}))\rangle &= \int_0^1 \left[\widetilde{r}(x)\nu_1^2(x,\mu_n(\hat{t})) - \widetilde{g}(x)\nu_2^2(x,\mu_n(\hat{t}))\right] dx \\ &= -\frac{it}{(4n+2)\pi}\int_0^1 [\widetilde{r}(x)-\widetilde{g}(x)]^2 dx \\ &+ \int_0^1 \frac{\widetilde{r}(x)-\widetilde{g}(x)}{2}[\cosh(2t\xi(x))\cos((2n+1)\pi x) \\ &+ i\sinh(2t\xi(x))\sin((2n+1)\pi x)]dx + O\left(\frac{1}{n^2}\right). \end{aligned}\tag{4.10}$$

This leads to

$$\begin{aligned}\int_0^1 \dot{\mu}_n(P_0+t\widetilde{P})dt &= \int_0^1 \frac{\langle \dot{\mathcal{A}}_2(\hat{t})\nu(x,\mu_n(\hat{t})), q(x,\overline{\mu_n}(\hat{t}))\rangle}{\langle \nu(x,\mu_n(\hat{t})), q(x,\overline{\mu_n}(\hat{t}))\rangle}dt \\ &= \int_0^1 \frac{\sinh(2\xi(x))}{4\xi(x)}[\widetilde{r}(x)-\widetilde{g}(x)]\cos((2n+1)\pi x)dx \\ &+ i\int_0^1 \frac{\cosh(2\xi(x))-1}{4\xi(x)}[\widetilde{r}(x)-\widetilde{g}(x)]\sin((2n+1)\pi x)dx \\ &- \frac{i}{(8n+4)\pi}\int_0^1 [\widetilde{r}(x)-\widetilde{g}(x)]^2 dx + O\left(\frac{1}{n^2}\right). \end{aligned}\tag{4.11}$$

The refinement of the asymptotic expression for $\mu_n(P)$ to $O(1/n^2)$ is now possible. Returning to (4.6), and using (2.14) and (4.11),

$$\begin{aligned}\mu_n(P) = \mu_n(P_0 + \widetilde{P}) &= \mu_n(P_0) + \int_0^1 \frac{d}{dt}\mu_n(P_0 + t\widetilde{P})dt \\ &= \frac{r_0 + g_0}{2} + \int_0^1 \frac{\sinh(2\xi(x))}{4\xi(x)}[\widetilde{r}(x) - \widetilde{g}(x)]\cos((2n+1)\pi x)dx \\ &\quad + \frac{i(2n+1)\pi}{2} - \frac{i}{(8n+4)\pi}\int_0^1 [r(x) - g(x)]^2 dx \\ &\quad + i\int_0^1 \frac{\cosh(2\xi(x)) - 1}{4\xi(x)}[\widetilde{r}(x) - \widetilde{g}(x)]\sin((2n+1)\pi x)dx + O\left(\frac{1}{n^2}\right). \quad (4.12)\end{aligned}$$

4.2 Verifying the Accuracy of the Expression for $\mu_n(P)$

To verify the accuracy of this expression, as was done for the expression for $\lambda_n(P)$, the eigenvalues computed from (4.12) are compared to the eigenvalues computed using the spectral discretization. (The spectral method used to calculate these eigenvalues is described in Chapter 7.) The functions $r(x) = 1 + x^2$ and $g(x) = x^2$ were used to generate the data in Table 4.1. The second column of the table shows the value for μ_n calculated with spectral discretization (using $N = 128$). For this r, g, and N, we believe the eigenvalues from the spectral method are exact to the digits listed. The third column of the table shows the values for μ_n calculated with the asymptotic expression in (4.12). (For asymptotic calculations, symbolic integration and evaluation were done with Mathematica.)

In the table, the underlined digits are exactly the same from spectral results and asymptotic results. As n increases, the spectral results and asymptotic results tend to agree to more digits, since the asymptotic expression is most accurate for large n. This can be seen in Figure 4.1, for $r(x) = 1 + x^2$ and $g(x) = x^2$, where the magnitude of the difference between the value computed with spectral discretization and the

Table 4.1 : Eigenvalues of $\mathcal{A}_2(P)$ when $r(x) = 1 + x^2$ and $g(x) = x^2$ calculated with spectral discretization, using $N = 128$, and with the asymptotic expression in (4.12). The underlined digits are exactly the same from spectral and asymptotic results.

n	spectral eigenvalue	asymptotic eigenvalue
0	0.8322372 + 1.55545i	0.8333333 + 1.49121i
1	0.8342449 + 4.68817i	0.8333333 + 4.68586i
2	0.8334586 + 7.83857i	0.8333333 + 7.83806i
3	0.8333667 +10.98439i	0.8333333 +10.98420i
4	0.8333456 +14.12841i	0.8333333 +14.12832i
5	0.8333388 +17.27157i	0.8333333 +17.27152i
6	0.8333361 +20.41426i	0.8333333 +20.41423i
7	0.8333349 +23.55665i	0.8333333 +23.55663i
8	0.8333343 +26.69886i	0.8333333 +26.69885i
9	0.8333339 +29.84095i	0.8333333 +29.84094i
10	0.8333337 +32.98294i	0.8333333 +32.98293i

asymptotic expression is plotted as n increases. The line in Figure 4.1 shows a rate of decrease of $1/n^2$. Since the dots are decreasing faster than this rate, it can be concluded that the asymptotic expression is actually more accurate than $O(1/n^2)$ in this example.

Returning to the refined asymptotic expression for the eigenvalues of $\mathcal{A}_1(P)$, in the next chapter, (3.55) will be used to derive an expression that can be used to recover information about resistance in the telegrapher's equation.

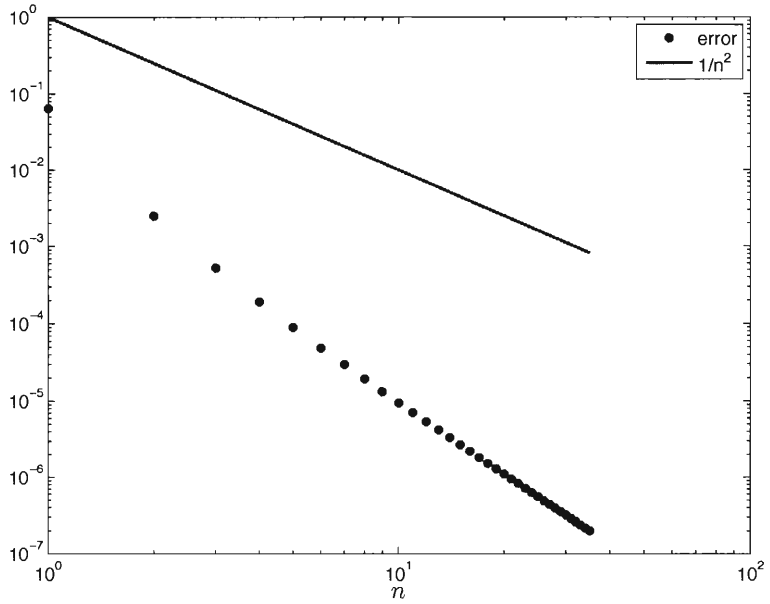

Figure 4.1 : This plot shows the decrease in the magnitude of the difference between μ_n of $\mathcal{A}_1(P)$ calculated with spectral discretization (using $N = 128$) and calculated with the asymptotic expression in (4.12) as n increases when $r(x) = 1 + x^2$ and $g(x) = x^2$.

Chapter 5

Inverse Spectral Problem for $\mathcal{A}_1(P)$

The inverse spectral problem for $\mathcal{A}_1(P)$, considered in this research, seeks the recovery of information about r and g, given information about the eigenvalues. Let

$$\phi(x) \equiv [\widetilde{r}(x) - \widetilde{g}(x)]\frac{\sinh(2\xi(x))}{4\xi(x)} \tag{5.1}$$

and

$$\psi(x) \equiv [\widetilde{r}(x) - \widetilde{g}(x)]\frac{\cosh(2\xi(x)) - 1}{4\xi(x)}, \tag{5.2}$$

which appear in the integrand of the real part and imaginary part, respectively, of the expression found for the eigenvalues, $\lambda_n(P)$, in (3.55).

The techniques in this thesis require that the functions to be recovered, r and g, are even. In this research, "even" means the function is symmetric about the midpoint, $x = 1/2$. If r and g are even, then $(r-g)/2$, $\widetilde{r}$, $\widetilde{g}$, and ϕ are also even. However, ξ and ψ are odd.

Arguing as in Cox and Embree's paper [3], since ϕ is even and ψ is odd, the nth Fourier coefficients for ϕ and ψ are

$$\int_0^1 \phi(x)\cos(2n\pi x)dx = \int_0^1 [\widetilde{r}(x) - \widetilde{g}(x)]\frac{\sinh(2\xi(x))}{4\xi(x)}\cos(2n\pi x)dx$$

and

$$\int_0^1 \psi(x)\sin(2n\pi x)dx = \int_0^1 [\widetilde{r}(x) - \widetilde{g}(x)]\frac{\cosh(2\xi(x)) - 1}{4\xi(x)}\sin(2n\pi x)dx.$$

Notice that these are precisely the integrals that arise in the asymptotic expression for $\lambda_n(P)$ in (3.55). So, knowledge of $\lambda_n(P)$ can give insight into ϕ and ψ. In particular,

ϕ and ψ can be expressed as

$$\phi(x) = \int_0^1 [\widetilde{r}(x) - \widetilde{g}(x)] \frac{\sinh(2\xi(x))}{4\xi(x)} dx + \\ + 2\sum_{n=1}^{\infty} \left[\mathrm{Re}(\lambda_n(P)) - \frac{r_0 + g_0}{2} + O\left(\frac{1}{n^2}\right) \right] \cos(2n\pi x) \quad (5.3)$$

and

$$\psi(x) = 2\sum_{n=1}^{\infty} \left[\mathrm{Im}(\lambda_n(P)) - n\pi + \frac{1}{8n\pi} \int_0^1 [r(x) - g(x)]^2 dx + O\left(\frac{1}{n^2}\right) \right] \sin(2n\pi x). \quad (5.4)$$

Given a finite set of eigenvalues, is it possible to recover ϕ and ψ from these expressions? The functions ϕ and ψ both clearly involve $\widetilde{r} - \widetilde{g}$, while ξ was defined in terms of $\widetilde{r} + \widetilde{g}$. It is possible to write an expression involving ϕ and ψ that uniquely determines ξ, so if ϕ and ψ can be recovered with sufficient accuracy, ϕ, ψ, and ξ could be used to recover r and g [3].

Unfortunately, similar to the results of Cox and Embree, while ϕ is recovered with good accuracy, ψ is not [3]. As Cox and Embree point out, this can be attributed to ψ being so small (in magnitude) for typical choices of r and g [3]. One example of this is shown in Figure 5.1 when $r(x) = 1$ and $g(x) = 1 + \sin(\pi x)$.

If ξ is sufficiently small, the following approximations can be made for ϕ and ψ:

$$\begin{aligned} \phi &= (\widetilde{r} - \widetilde{g}) \frac{\sinh(2\xi)}{4\xi} \\ &= (\widetilde{r} - \widetilde{g}) \left[\frac{2\xi + (2\xi)^3/6 + O(|\xi|^5)}{4\xi} \right] \\ &= (\widetilde{r} - \widetilde{g}) \left[\frac{1}{2} + \frac{\xi^2}{3} + O(|\xi|^4) \right] \end{aligned} \quad (5.5)$$

and

$$\begin{aligned}\psi &= (\widetilde{r}-\widetilde{g})\frac{\cosh(2\xi)-1}{4\xi} \\ &= (\widetilde{r}-\widetilde{g})\left[\frac{1+(2\xi)^2/2+(2\xi)^4/24+O(|\xi|^6)-1}{4\xi}\right] \\ &= (\widetilde{r}-\widetilde{g})\left[\frac{\xi}{2}+\frac{\xi^3}{6}+O(|\xi|^5)\right]. \end{aligned} \tag{5.6}$$

Therefore,

$$\phi = \frac{1}{2}(\widetilde{r}-\widetilde{g}) + O\left(\| \widetilde{r}-\widetilde{g} \|_{L^\infty} \| \xi^2 \|_{L^\infty}\right) \approx \frac{\widetilde{r}-\widetilde{g}}{2}$$

and

$$\psi = O\left(\| \widetilde{r}-\widetilde{g} \|_{L^\infty} \| \xi \|_{L^\infty}\right) \approx 0.$$

So, for a finite set of m eigenvalues, $\lambda_1, ..., \lambda_m$,

$$\frac{r(x)-g(x)}{2} \approx \frac{r_0-g_0}{2} + 2\sum_{j=1}^{m}\left[\mathrm{Re}(\lambda_j(P)) - \frac{r_0+g_0}{2}\right]\cos(2j\pi x)$$

or

$$\frac{\widetilde{r}(x)-\widetilde{g}(x)}{2} \approx 2\sum_{j=1}^{m}\left[\mathrm{Re}(\lambda_j(P)) - \frac{r_0+g_0}{2}\right]\cos(2j\pi x). \tag{5.7}$$

Figure 5.1 shows an example of the recovery of $(\widetilde{r}-\widetilde{g})/2$ when $r(x) = 1$ and $g(x) = 1+\sin(\pi x)$. Results for a variety of r and g are presented in Chapter 6.

In the top row of graphs in Figure 5.1, r and g are plotted in the left graph. The middle graph shows ξ. The right graph on the first row shows the eigenvalues with non-negative imaginary part computed using spectral discretization with $N = 128$.

For this example and the other results in Chapter 6, in the code to recover the functions, the real part of the m-th eigenvalue (the eigenvalue with the largest magnitude used in the recovery) is used to approximate the value of $(r_0+g_0)/2$. For these recovered graphs, $m = 10$ eigenvalues were used, and only eigenvalues with nonzero imaginary part were used in the recovery.

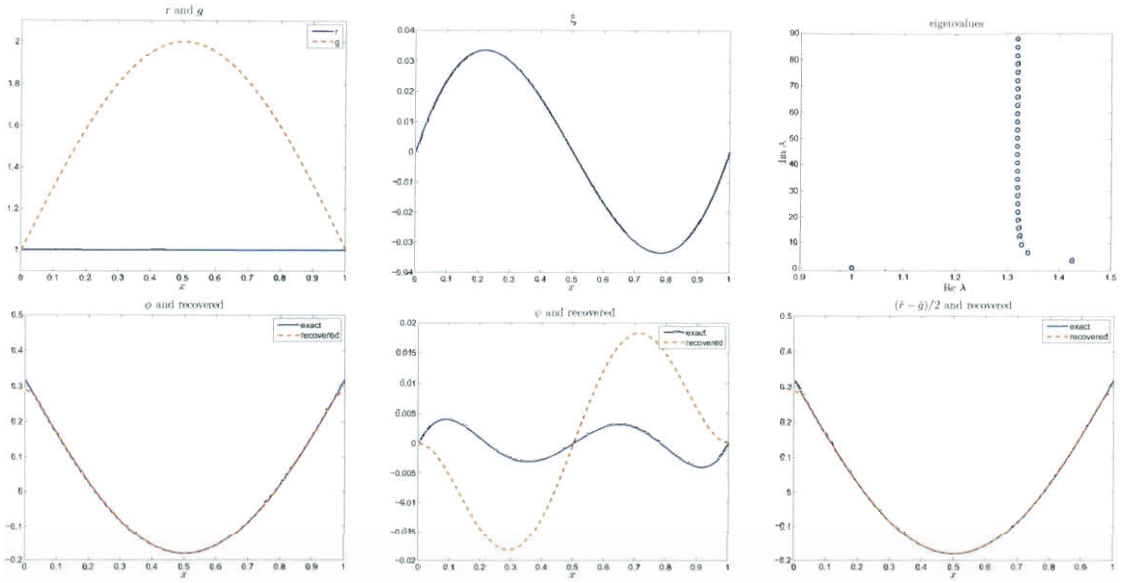

Figure 5.1 : The exact and recovered graphs when $r(x) = 1$ and $g(x) = 1 + \sin(\pi x)$ when $N = 128$ and $m = 10$.

The left graph on the second row shows the exact ϕ and the recovered ϕ using (5.3), and the middle graph shows the exact ψ and the recovered ψ using (5.4). This example shows that ϕ is recovered quite accurately, while ψ is not. These results are typical of the other choices of r and g used in the examples in Chapter 6. The graph on the right shows $(\widetilde{r} - \widetilde{g})/2$ exactly and the recovered $(\widetilde{r} - \widetilde{g})/2$ from (5.7), which shows $(\widetilde{r} - \widetilde{g})/2$ is recovered quite accurately.

Chapter 6

Results for $\mathcal{A}_1(P)$

In this chapter, I report the results collected from choosing various (even) r and g, finding the eigenvalues of the resulting operator $\mathcal{A}_1(P)$, then recovering $(\widetilde{r} - \widetilde{g})/2$.

For the results in this chapter, in the code to recover $(\widetilde{r} - \widetilde{g})/2$, the real part of the m-th eigenvalue (the eigenvalues with the largest magnitude used in the recovery) is used to approximate the value of $(r_0 + g_0)/2$.

6.1 How Many Eigenvalues are Needed to Accurately Recover $(\widetilde{r} - \widetilde{g})/2$?

In this section, various r and g are chosen, and the results are compared when various numbers of eigenvalues are used in the recovery of $(\widetilde{r} - \widetilde{g})/2$.

For the first examples in this section, r or g is chosen to be a constant 1, and the other is a continuous, non-constant function, each more complicated than the previous. The last example in this section has r and g chosen so that $r - g$ is constant.

6.1.1 r or g is 1

1. For this first example, the same functions used for Figure 5.1 (in the previous chapter) will be used: $r(x) = 1$ and $g(x) = 1 + \sin(\pi x)$, a smoothly changing function with one maximum at $x = 1/2$.

In Figure 5.1, r and g are plotted in the top left graph, and the top right graph shows the eigenvalues with non-negative imaginary part calculated using spectral discretization. For this and all other examples in this chapter, $N = 128$ was used in the spectral discretization, unless otherwise specified. The eigenvalues for this example are already almost in a vertical line in the complex plane when n is fairly small, approximately $n = 5$. The bottom left graph in Figure 5.1 shows the exact ϕ and the recovered ϕ using (5.3), while the graph on the bottom right shows $(\widetilde{r} - \widetilde{g})/2$ exactly and the recovered $(\widetilde{r} - \widetilde{g})/2$ from (5.7). For all of the recovered graphs in this chapter, $m = 10$ eigenvalues were used in the recovery, unless otherwise specified.

Included in this chapter are additional graphs for this example. The left graph in Figure 6.1 shows $(\widetilde{r} - \widetilde{g})/2$ and approximations from using various values of m. The middle graph is a close up view of the top left corner of the left graph. The graph on the right is a plot of the maximum of the absolute value of the difference between $(\widetilde{r} - \widetilde{g})/2$ and the recovered approximation for various values of m. (This plot, and most others in this chapter, stops at $m = 35$ because that is how many eigenvalues converged to high precision with $N = 128$.)

From this example, and the other examples in this section, it can been seen that the recovered $(\widetilde{r} - \widetilde{g})/2$ matches the exact $(\widetilde{r} - \widetilde{g})/2$ well when $m = 10$ eigenvalues are used in the recovery.

If $g(x) = 1$ and $r(x) = 1 + \sin(\pi x)$, the resulting graphs are not significantly different from these shown here. The main difference seen in the plots if $g(x) = 1$ and $r(x) = 1 + \sin(\pi x)$ (compared to the plots shown here) is that the graph of the eigenvectors has been reflected across the vertical line the eigenvalues are

approaching as n goes to infinity.

2. In this example, $r(x) = 1$ and g has 3 maxima and the change is very steep,

$$g(x) = 1 + \frac{1}{2}\sum_{j=1}^{3} \exp\left(-256\left(x - \frac{j}{4}\right)^2\right).$$

The graphs for this example are in Figure 6.2, and, corresponding figures will show for all the other examples in this chapter, in the left graph r and g are plotted. The second graph, from left to right, shows the eigenvalues with non-negative imaginary part calculated using spectral discretization. The eigenvalues for this example do not begin approaching a vertical line as quickly as the previous example. The third graph from the left shows the exact ϕ and the recovered ϕ using (5.3). The graph on the right shows $(\widetilde{r} - \widetilde{g})/2$ exactly and the recovered $(\widetilde{r} - \widetilde{g})/2$ from (5.7).

The left graph in Figure 6.3 shows $(\widetilde{r} - \widetilde{g})/2$ and approximations from using various values of m. The graph on the right is a plot of the maximum of the absolute value of the difference between $(\widetilde{r} - \widetilde{g})/2$ and the recovered approximation for various values of m. The error decreases very differently for this example than it did for the previous example.

When r and g are switched, the resulting graphs show the same behavior described in the previous example.

3. In this example, $g(x) = 1$ and $r(x)$ is discontinuous,

$$r(x) = \begin{cases} 1.5, & 1/3 < x < 2/3, \\ 2, & \text{otherwise.} \end{cases}$$

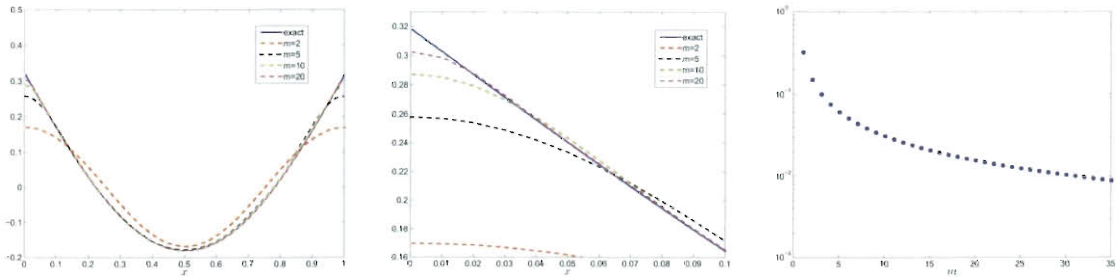

Figure 6.1 : When $r(x) = 1$ and $g(x) = 1 + \sin(\pi x)$, recovery of $(\widetilde{r} - \widetilde{g})/2$ using m eigenvalues, for various m.

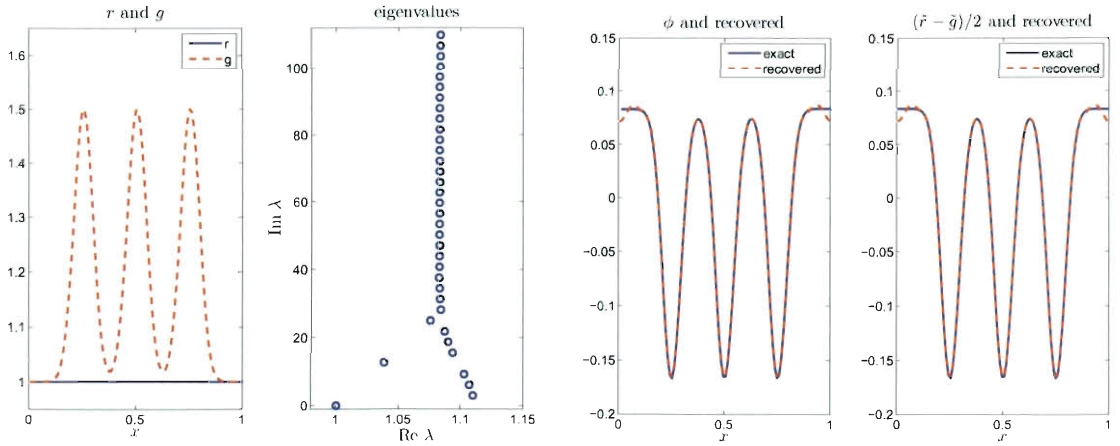

Figure 6.2 : The exact and recovered graphs when $r(x) = 1$ and g has 3 maxima and the change is very steep with $N = 128$ and $m = 10$.

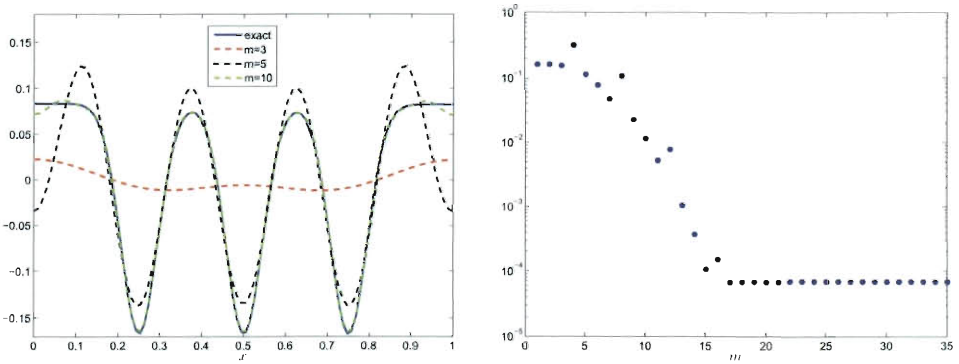

Figure 6.3 : When $r(x) = 1$ and g has 3 maxima and the change is very steep, recovery of $(\widetilde{r} - \widetilde{g})/2$ using m eigenvalues, for various m.

The results in Figure 6.4 were generated using $N = 512$ in the spectral discretization.

In Figure 6.4, the eigenvalues for this example show a great deal of movement. Even when $n = 28$ and $\mathrm{Im}(\lambda_{28}) \approx 90$, the eigenvalues have not settled down into a vertical line like the previous two examples did for much smaller values of n. The amount of deviation from a vertical line is noticed more when the scale of the graph is compared to the previous examples. Also, in this example, there is no real eigenvalue.

In Figure 6.5, the graph on the right shows the maximum of the absolute value of the difference between $(\widetilde{r}-\widetilde{g})/2$ and the recovered function as m increases for two different N. This plot shows a trend of increase in the error as m increases for $N = 128$. That is why $N = 512$ was used to generate the results in Figures 6.4, 6.5, 6.6, and 6.7.

It is not surprising that the results do not show the same accuracy when one function is discontinuous compared to the previous examples when r and g were both continuous. Other methods, such as spectral element, would work better for discontinuous functions, but the accuracy obtained with this method is sufficient for the purposes of this research.

4. In this example, $r(x) = 1$ and $g(x)$ is discontinuous,

$$g(x) = \begin{cases} 1.75, & 1/4 < x < 3/4, \\ 1, & \text{otherwise.} \end{cases}$$

The results in Figure 6.6 were generated using $N = 512$ in the spectral discretization, for the same reasons that were mentioned in the previous example.

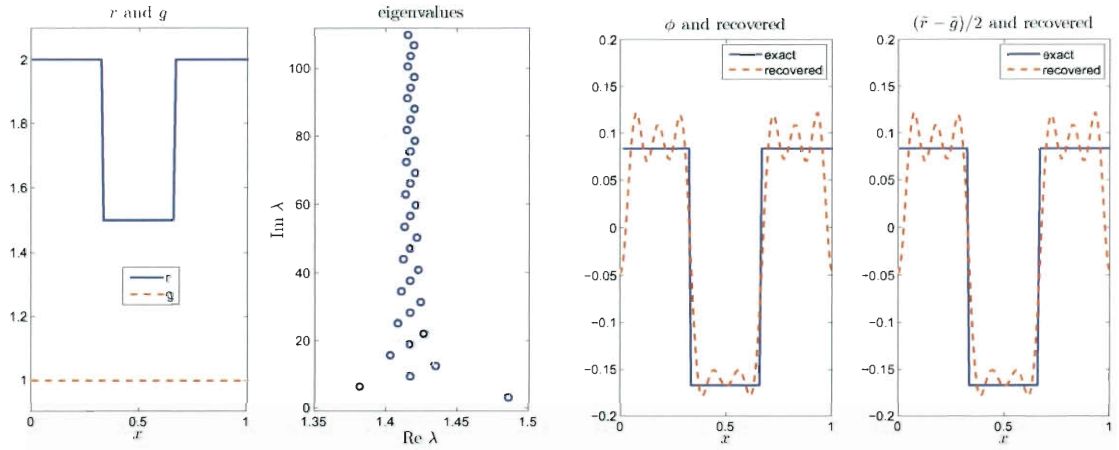

Figure 6.4 : The exact and recovered graphs when $g(x) = 1$ and r is discontinuous with $N = 512$ and $m = 10$.

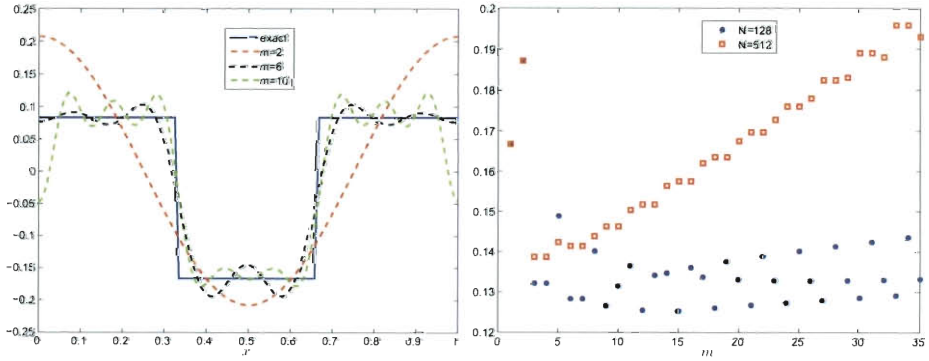

Figure 6.5 : When $g(x) = 1$ and r is discontinuous, recovery of $(\widetilde{r} - \widetilde{g})/2$ using m eigenvalues, for various m.

The behavior of the eigenvalues for this example is similar to the previous example, when r was discontinuous, except for this example, there is a real eigenvalue.

The left graph in Figure 6.7 shows $(\widetilde{r} - \widetilde{g})/2$ and approximations from using various values of m. The graph on the right shows the rate of decrease of the maximum of the absolute value of the difference between $(\widetilde{r} - \widetilde{g})/2$ and the recovered function as m increases.

For all examples in this subsection, when different constants, such as $1/2$ and 2, were used in the various examples, the eigenvalues and the recovered graphs only changed slightly.

6.1.2 $r - g$ is Constant

1. For the last example in this section, $g(x) = 1 + \sin(\pi x)$ and $r(x) = 2 + \sin(\pi x)$, so that $r - g$ is a constant 1.

   In Figure 6.8, except for the real eigenvalue, these eigenvalues are in a vertical line. While the recovery of ϕ and $(\widetilde{r} - \widetilde{g})/2$ do not appear very accurate with this scale, the plot on the right in Figure 6.9 shows the error in this recovery is similar to what has been seen in the other examples.

   The left graph in Figure 6.9 shows $(\widetilde{r} - \widetilde{g})/2$ and approximations from using various values of m. Graphs using $m > 5$ were basically indistinguishable from the plot with $m = 5$, on this scale, so they were not included in this plot. The graph on the right shows a plot of the maximum of the absolute value of the difference between $(\widetilde{r} - \widetilde{g})/2$ and the recovered approximation for various values of m. This plot shows the best approximation, using this definition of error,

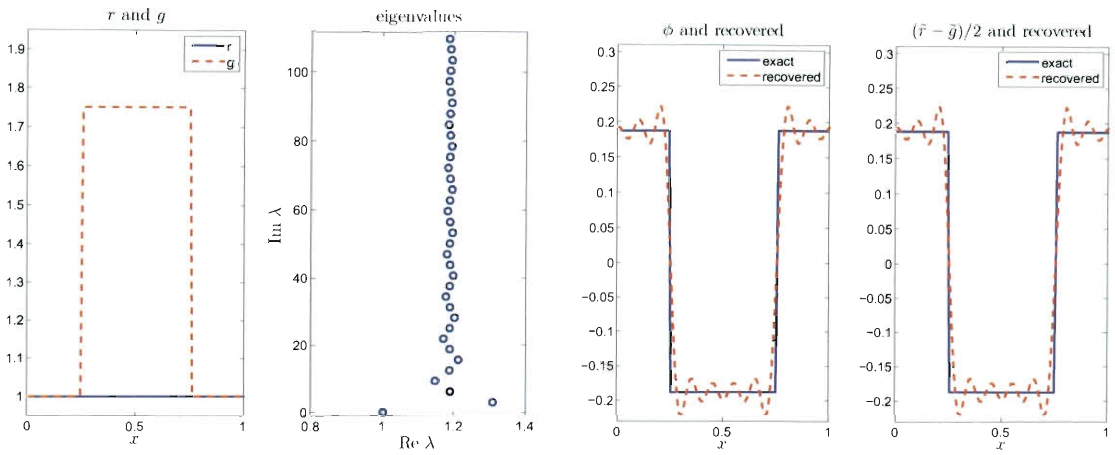

Figure 6.6 : The exact and recovered graphs when $r(x) = 1$ and g is discontinuous with $N = 512$ and $m = 10$.

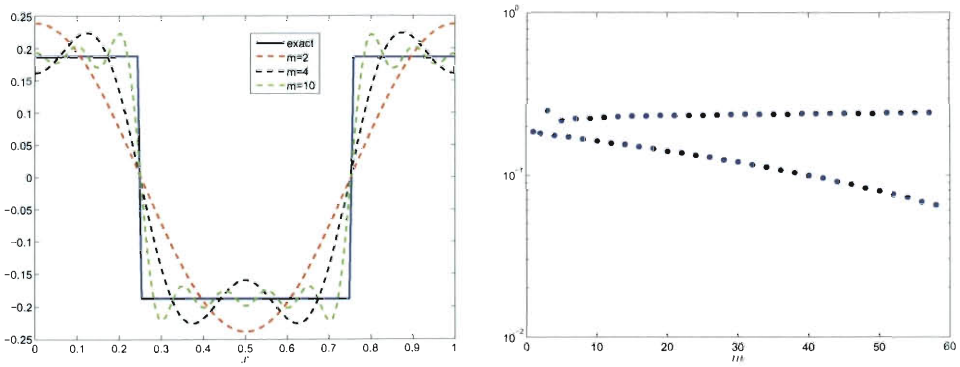

Figure 6.7 : When $r(x) = 1$ and g is discontinuous, recovery of $(\widetilde{r} - \widetilde{g})/2$ using m eigenvalues, for various m.

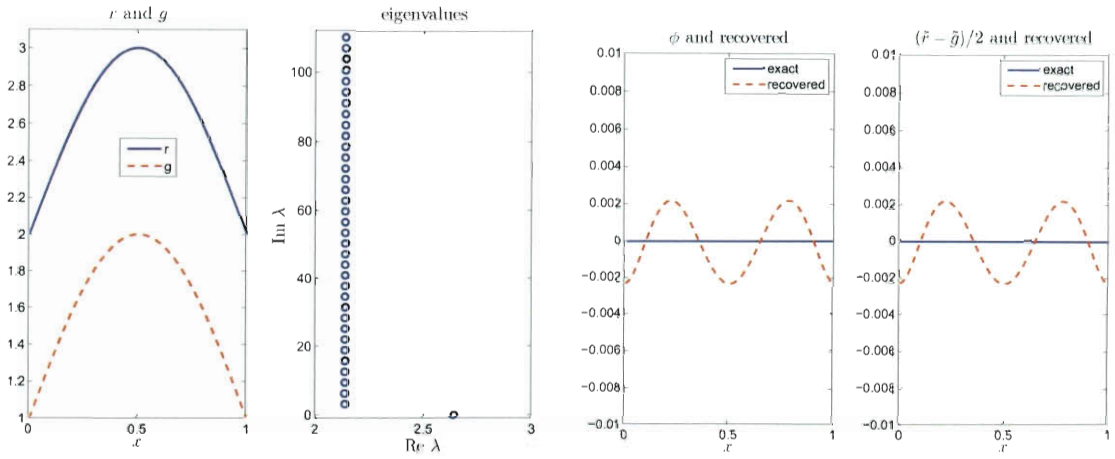

Figure 6.8 : The exact and recovered graphs when $g(x) = 1 + \sin(\pi x)$ and $r(x) = 2 + \sin(\pi x)$ with $N = 128$ and $m = 10$.

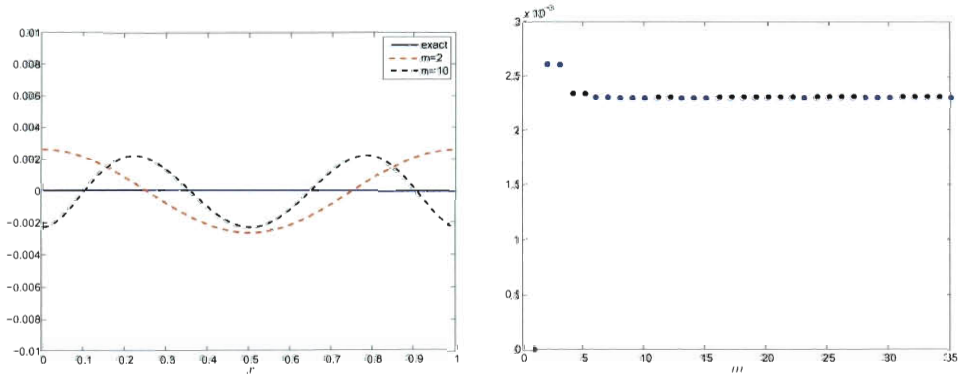

Figure 6.9 : When $g(x) = 1 + \sin(\pi x)$ and $r(x) = 2 + \sin(\pi x)$, recovery of $(\widetilde{r} - \widetilde{g})/2$ using m eigenvalues, for various m.

is achieved when only one eigenvalue is used in the recovery. If more than one eigenvalue is going to be used in the recovery, there is virtually no difference, in this measurement of error, when using 2 eigenvalues or 15 eigenvalues.

6.2 Various Examples

6.2.1 r or g is Constant

Since the graphs of exact and recovered ϕ are basically the same as exact and recovered $(\widetilde{r} - \widetilde{g})/2$, instead of showing both, for the rest of the chapter, only the exact and recovered $(\widetilde{r} - \widetilde{g})/2$ will be shown.

1. In this example, $r(x) = 1$ and $g(x) = 1 + \exp(-256(x - 1/2)^2)$, which has 1 maximum with a very steep change.

   In Figure 6.10, on the left, again, r and g are plotted. The eigenvalues are plotted in the second graph, and for this example, they can be seen to fall differently than for the previous examples. Now, the third graph shows the exact $(\widetilde{r} - \widetilde{g})/2$ and the recovered $(\widetilde{r} - \widetilde{g})/2$ from (5.7). The graph on the right shows the absolute value of the difference between the exact $(\widetilde{r} - \widetilde{g})/2$ and the recovered $(\widetilde{r} - \widetilde{g})/2$.

   When the height of the maximum in g is decreased to $1/2$, the results are basically the same, except the horizontal spread of the eigenvalues is decreased.

2. In this example, $r(x) = 1$ and g has 3 maxima and 2 minima and the change is very steep,

$$g(x) = 1 + \frac{1}{2}\sum_{j=1}^{3} \exp\left(-256\left(x - \frac{j}{4}\right)^2\right) - \frac{1}{2}\sum_{j=1}^{2} \exp\left(-256\left(x - \frac{2j+1}{8}\right)^2\right).$$

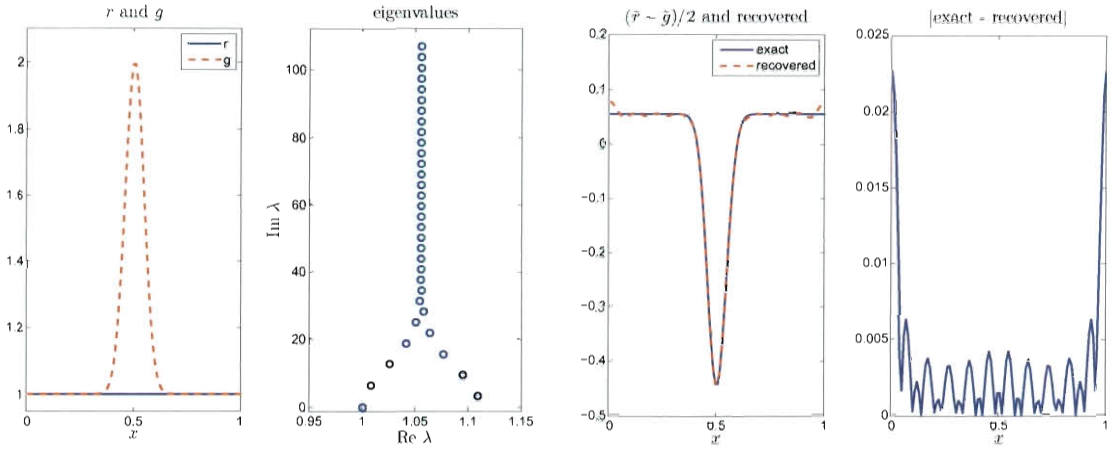

Figure 6.10 : The exact and recovered graphs when $r(x) = 1$ and $g(x) = 1 + \exp(-256(x - 1/2)^2)$ with $N = 128$ and $m = 10$.

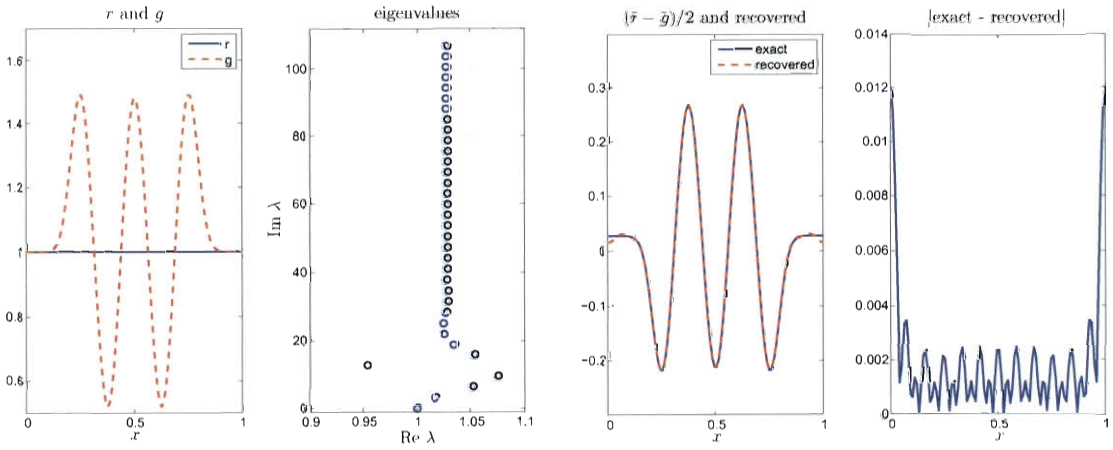

Figure 6.11 : The exact and recovered graphs when $r(x) = 1$ and $g(x)$ has 3 maxima and 2 minima using $N = 128$ and $m = 10$.

The eigenvalues for this example exhibit different behavior from the previous examples before settling down to approach a vertical line.

3. In this example, the effect of having more than one pure real eigenvalue will be illustrated.

   If $r(x) = 6 + \sin(\pi x)$ and $g(x) = 0.15$, there is only one real eigenvalue.

   In Figure 6.12, because r and g are so far apart, the recovery of $(\widetilde{r} - \widetilde{g})/2$ is not as accurate as in the previous examples.

   If r stays the same, but $g(x) = 0.14$, there are three real eigenvalues. Initially the code to recover $(\widetilde{r} - \widetilde{g})/2$ simply ignored the first eigenvalue produced by the spectral discretization, assuming it was real (because the eigenvalues had been sorted by imaginary part). This caused problems in the recovery of $(\widetilde{r} - \widetilde{g})/2$ for choices of r and g such as this one, when there are more than one real eigenvalue, and for other problems when there are no real eigenvalues produced (an example of this was mentioned in the previous section).

   When an eigenvalue was incorrectly excluded or included, the recovered graphs did not agree with the exact graphs, similar to what is seen in Figure 6.13. Notice the very different scale on the vertical axis of the two right graphs, compared to the scales of the graphs in Figure 6.12.

   When all three real eigenvalues are ignored, the recovered $(\widetilde{r} - \widetilde{g})/2$ is shown in Figure 6.14. This recovery is not as accurate as the other examples listed in this thesis, but it is closer than what is shown in Figure 6.13.

6.2.2 Neither r nor g is Constant

1. In this example, $g(x) = 1 + \sin(\pi x)$ and $r(x) = 1 - \sin(\pi x)$.

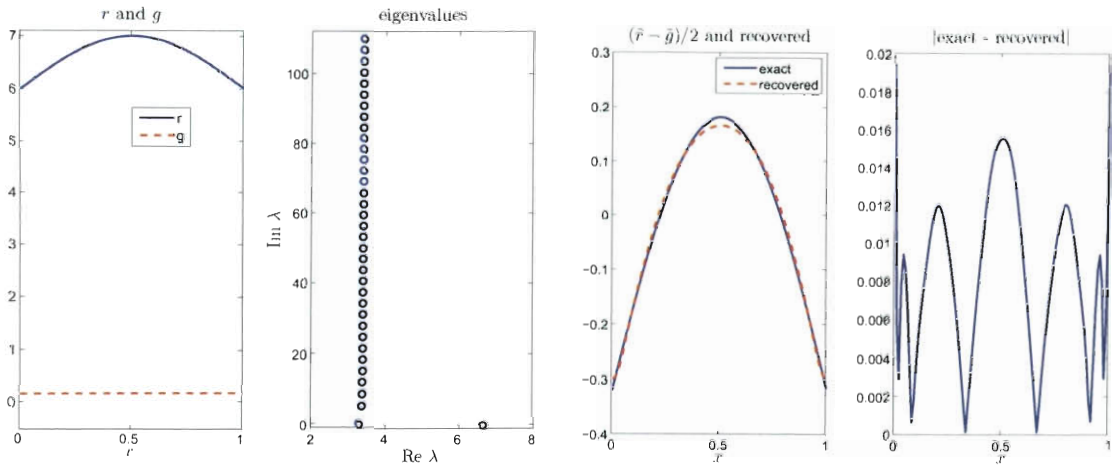

Figure 6.12 : The exact and recovered graphs when $r(x) = 6+\sin(\pi x)$ and $g(x) = 0.15$ with $N = 128$ and $m = 10$.

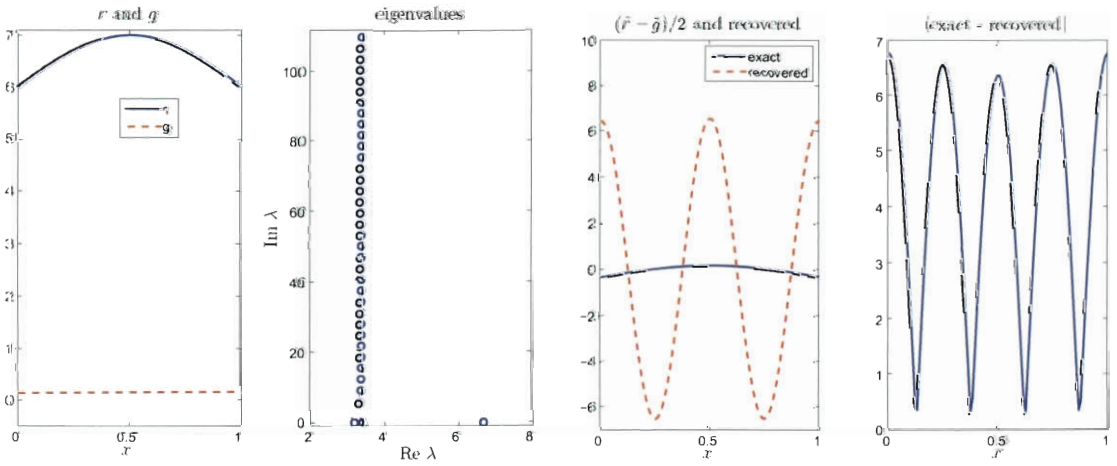

Figure 6.13 : The exact and recovered graphs when $r(x) = 6+\sin(\pi x)$ and $g(x) = 0.14$, including real eigenvalues.

For these particular functions, $\xi(x) = 0$, but $(\widetilde{r} - \widetilde{g})/2$ is still recovered with good accuracy, as seen in Figure 6.15.

When $g(x) = 1 + \sin(\pi x)$ and $r(x) = 2 - \sin(\pi x)$, the results are similar.

6.3 A Problem to Imitate Finding a Fault on a Submarine Cable

6.3.1 One Fault in the Middle of the Cable

In an effort to apply the technique determined in this thesis to recover unknown resistance from the telegrapher's equation to a real-world type problem, imagine a situation with an idealized uniform submarine telegraph cable of unit length. The capacitance and inductance of the cable are one, known from design and manufacturing. The resistance and leakage conductance are known to be $r(x) = r_{und}$ and $g(x) = g_{und}$, respectively, again known from design and manufacturing, if the cable is undamaged and installed properly.

Imagine further that the cable is installed properly through some body of water. After some time, the insulation of the cable is damaged in some way (a fisherman uses a stick of dynamite to "catch" fish in the body of water, and the dynamite detonates close enough to the cable to damage it; the cable gets caught in regular fishing nets and is dragged over sharp rocks which damage the insulation of the cable before the net stops dragging the cable; a shark, or some other sea creature, bites the cable, or damages it in some way; or an iceberg travels over where the line was laid, and the insulation of the line is damaged [14]).

Since the technique in this thesis requires the functions r and g to be even, further imagine the damage occurs perfectly centered around the midpoint of the cable for

some unknown length, $2d$. The resulting damage causes $r(x)$ to change immediately by some unknown, but constant, value r_{dam} and $g(x)$ to instantly change by some unknown constant g_{dam} for the length $2d$ centered around $x = 1/2$.

If the eigenvalues from this situation can be obtained, how accurately can d, r_{dam}, and g_{dam} be determined?

For a specific instance of this example, after the damage has occurred, let

$$g(x) = g_{und} + (\chi_{1/2\pm d})g_{dam} = \begin{cases} 1.75, & 1/4 < x < 3/4, \\ 1, & \text{otherwise}, \end{cases}$$

and

$$r(x) = r_{und} + (\chi_{1/2\pm d})r_{dam} = \begin{cases} 1.5, & 1/4 < x < 3/4, \\ 2, & \text{otherwise}. \end{cases}$$

The results of my MATLAB code to recover $(\widetilde{r} - \widetilde{g})/2$ are shown in Figure 6.16 using $N = 128$ and $m = 10$. (The choice was made to use $N = 128$ rather than $N = 512$, as in the previous examples when one function was discontinuous, to examine how successfully $(\widetilde{r} - \widetilde{g})/2$ could be recovered by this method with less than ideal eigenvalues. The following calculations were made when $N = 512$ was used, and the final answers differed from these presented by less than one tenth.)

For this situation,

$$\begin{aligned} r_0 &= \int_0^1 r(x)dx = r_{und} + 2dr_{dam} = 7/4 \\ g_0 &= \int_0^1 g(x)dx = g_{und} + 2dg_{dam} = 11/8. \end{aligned} \tag{6.1}$$

Therefore,

$$\frac{r_0 + g_0}{2} = \frac{r_{und} + g_{und}}{2} + d(r_{dam} + g_{dam}). \tag{6.2}$$

Also,

$$\widetilde{r}(x) = r(x) - r_0 = (\chi_{1/2\pm d})r_{dam} - 2dr_{dam}$$
$$\widetilde{g}(x) = g(x) - g_0 = (\chi_{1/2\pm d})g_{dam} - 2dg_{dam}. \tag{6.3}$$

Therefore,

$$\frac{\widetilde{r}(x) - \widetilde{g}(x)}{2} = \frac{r_{und} - g_{und}}{2} + \frac{g_0 - r_0}{2} + (\chi_{1/2\pm d})\frac{r_{dam} - g_{dam}}{2}. \tag{6.4}$$

Given the eigenvalues, it will be shown how one can use the graph of the recovered $(\widetilde{r} - \widetilde{g})/2$, along with the estimate for $(r_0 + g_0)/2$, to recover the unknown r_{dam}, g_{dam}, and d with reasonable accuracy.

The recovered approximation for $(\widetilde{r} - \widetilde{g})/2$ using $m = 10$ eigenvalues is plotted with a grid in Figure 6.17. From this graph, an approximate value for d can be deduced from the points of discontinuity; cf. (6.4). From this graph, it is reasonable to conclude that d is approximately $1/4$. It still remains to recover r_{dam} and g_{dam}.

As before, the real part of the m-th eigenvalue (the eigenvalue with largest magnitude used in the recovery) approximates $(r_0 + g_0)/2$, and so $(r_0 + g_0)/2 \approx 1.5652$. The exact value of $(r_0 + g_0)/2$ for this problem is 1.5625, so this approximation is quite good.

To finish recovering r_{dam} and g_{dam}, two data points are needed from the recovered graph for $(\widetilde{r}(x) - \widetilde{g}(x))/2$, one from a damaged interval and one from an undamaged interval. For this example, it would be reasonable to choose one data point near $x = 1/2$ and one data point far enough away from $x = 1/2$ to be in the undamaged portion of the cable.

Because of the oscillations in the recovered graph, a choice could be made to average the maxima and minima to arrive at the data point to be used to find r_{dam}

and g_{dam}. Another possibility could be to simply attempt to approximate, as closely as possible, the middle point between the maximum and minimum on the graph. The data chosen from the graph in Figure 6.17 is highlighted on the graph and listed in Table 6.1 for the two techniques.

Table 6.1 : Data for the selected values from Figure 6.17.

x	y
0.0909	0.3419
0.1212	0.3133
0.1414	0.2848
0.4444	−0.2887
0.4747	−0.3081
0.5051	−0.3275

If the second method is chosen (simply trying to find the middle between the maximum and the minimum), substituting the data from the graph and the specific values for r_{und} and g_{und} for this problem into (6.4) results in

$$\frac{\widetilde{r}(0.1212) - \widetilde{g}(0.1212)}{2} = 0.3133 = \frac{1}{2} + \frac{g_0 - r_0}{2} \tag{6.5}$$

and

$$\frac{\widetilde{r}(0.4747) - \widetilde{g}(0.4747)}{2} = -0.3081 = \frac{1}{2} + \frac{g_0 - r_0}{2} + \frac{r_{dam} - g_{dam}}{2}. \tag{6.6}$$

Substituting the known values for r_{und} and g_{und} and the approximated values for d and $(r_0 + g_0)/2$ into (6.2) results in

$$1.5652 = \frac{3}{2} + \frac{1}{4}(r_{dam} + g_{dam}). \tag{6.7}$$

From (6.5), $(g_0 - r_0)/2 = -0.1876$, so from (6.6), $r_{dam} - g_{dam} = -1.2428$. From (6.7), $r_{dam} + g_{dam} = 0.2608$. Therefore, the recovered approximate values for r_{dam} and g_{dam} are $r_{dam} \approx -0.4910$ and $g_{dam} \approx 0.7518$, which are quite close to the exact values of -0.5 and 0.75, respectively.

6.3.2 More Than One Fault in the Cable

What if, instead of one damaged interval, there is more than one damaged interval? This technique is able recover information about the location and length of the damage along with the constants r_{dam} and g_{dam}, if the assumption of r and g being even is preserved.

A specific example of this is given here for a line that has been damaged on two intervals. In this case,

$$g(x) = \begin{cases} 1.75, & x \in (1/8, 3/8) \cup (5/8, 7/8), \\ 1, & \text{otherwise}, \end{cases}$$

$$= \begin{cases} g_{und} + g_{dam}, & x \in (1/2 - d_1, 1/2 - d_2) \cup (1/2 + d_2, 1/2 + d_1), \\ g_{und}, & \text{otherwise}, \end{cases}$$

and

$$r(x) = \begin{cases} 1.5, & x \in (1/8, 3/8) \cup (5/8, 7/8), \\ 2, & \text{otherwise}, \end{cases}$$

$$= \begin{cases} r_{und} + r_{dam}, & x \in (1/2 - d_1, 1/2 - d_2) \cup (1/2 + d_2, 1/2 + d_1), \\ r_{und}, & \text{otherwise}. \end{cases}$$

The values of r_0 and g_0 are unchanged from the previous example; therefore, the exact value of $(r_0 + g_0)/2 = 1.5625$ is also unchanged. However, equation (6.2) becomes

$$\frac{r_0 + g_0}{2} = \frac{r_{und} + g_{und}}{2} + (d_1 + d_2)(r_{dam} + g_{dam}). \tag{6.8}$$

Equation (6.4) becomes, for this specific example,

$$\frac{\widetilde{r}(x)-\widetilde{g}(x)}{2}=\begin{cases}\frac{r_{und}-g_{und}}{2}+\frac{g_0-r_0}{2}+\frac{r_{dam}-g_{dam}}{2}, & x\in(\frac{1}{8},\frac{3}{8})\cup(\frac{5}{8},\frac{7}{8}),\\ \frac{r_{und}-g_{und}}{2}+\frac{g_0-r_0}{2}, & \text{otherwise.}\end{cases} \tag{6.9}$$

The resulting graphs from the MATLAB code are shown in Figure 6.18, using $N = 128$ and $m = 10$ as in the previous example.

Approximating the values of d_1 and d_2 from the recovered graph of $(\widetilde{r}-\widetilde{g})/2$ leads to $d_1 \approx 0.3794$ and $d_2 \approx 0.1332$, which are still quite close to the actual values of $d_1 = 0.375$ and $d_2 = 0.125$. (The data collected from the graph for these approximations is listed in Table 6.2 and is shown in Figure 6.19.) The recovery yields an approximation of $(r_0+g_0)/2 \approx 1.6020$, which is not too far from the actual value of 1.5625. The next step in the process is to choose two values from the recovered graph of $(\widetilde{r}-\widetilde{g})/2$, one from a damaged interval and one from an undamaged interval. Substituting the data from the graph and the specific values for r_{und} and g_{und} for this problem into (6.9) results in

$$\frac{\widetilde{r}(0.4975)-\widetilde{g}(0.4975)}{2}=0.3488=\frac{1}{2}+\frac{g_0-r_0}{2} \tag{6.10}$$

and

$$\frac{\widetilde{r}(0.2965)-\widetilde{g}(0.2965)}{2}=-0.279=\frac{1}{2}+\frac{g_0-r_0}{2}+\frac{r_{dam}-g_{dam}}{2}. \tag{6.11}$$

Substituting the known values for r_{und} and g_{und} and the approximated values for d_1, d_2, and $(r_0+g_0)/2$ into (6.8) results in

$$1.6020=\frac{3}{2}+0.5126(r_{dam}+g_{dam}). \tag{6.12}$$

From (6.10), $(g_0-r_0)/2 = -0.1512$, so from (6.11), $r_{dam}-g_{dam} = -1.2556$. From (6.12), $r_{dam}+g_{dam} = 0.1990$. Therefore, the recovered approximate values for r_{dam}

Table 6.2 : Data for the selected values from Figure 6.19.

x	y
0.1206	−0.0007
0.3668	−0.0194
0.2764	−0.2301
0.2965	−0.279
0.3216	−0.3491
0.4221	0.3889
0.4673	0.3387
0.4975	0.3488

and g_{dam} are $r_{dam} \approx -0.5286$ and $g_{dam} \approx 0.7273$, which are not too far from the exact values of -0.5 and 0.75, respectively.

These results could be improved by using $N = 512$ in the spectral discretization, but these results are presented to show the effectiveness of this technique even with imperfect information about the eigenvalues.

In the next chapter, I describe the techniques I used to calculate the eigenvalues and eigenvectors presented in this thesis.

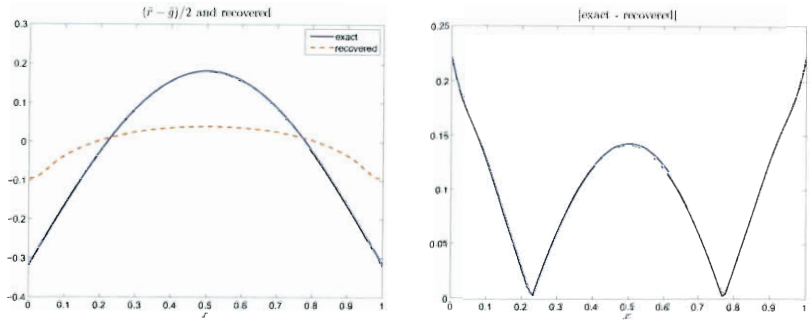

Figure 6.14 : The exact and recovered graphs when $r(x) = 6+\sin(\pi x)$ and $g(x) = 0.14$, excluding real eigenvalues.

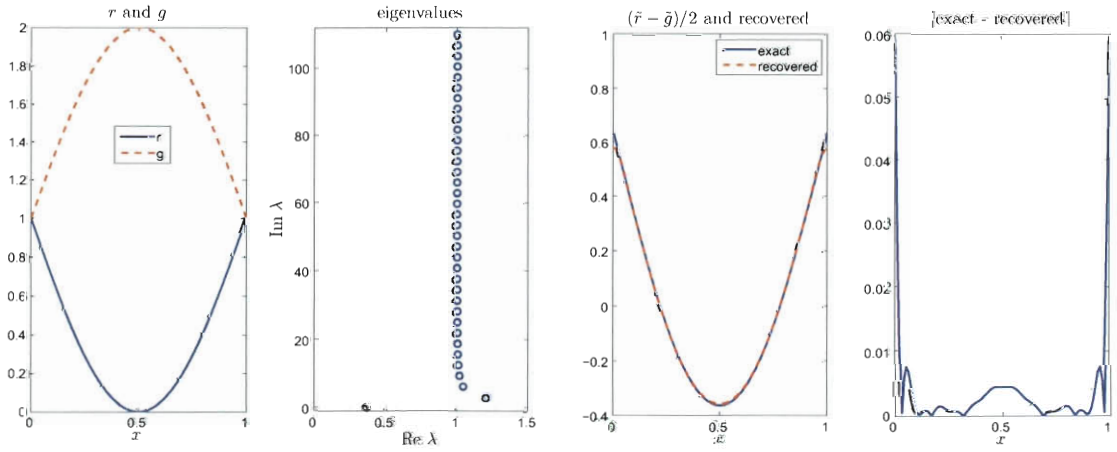

Figure 6.15 : The exact and recovered graphs when $g(x) = 1 + \sin(\pi x)$ and $r(x) = 1 - \sin(\pi x)$ with $N = 128$ and $m = 10$.

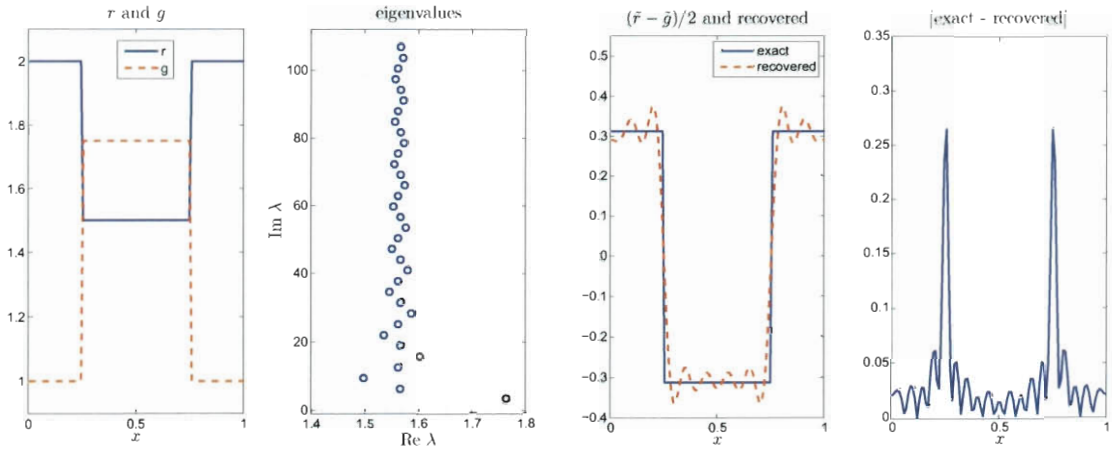

Figure 6.16 : The exact and recovered graphs when both r and g are discontinuous, with $N = 128$ and $m = 10$.

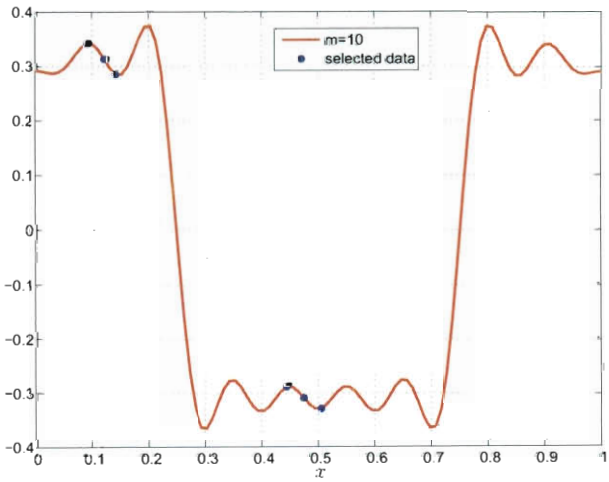

Figure 6.17 : Selected data from the recovery of $(\widetilde{r} - \widetilde{g})/2$, using $m = 10$, when r and g are discontinuous.

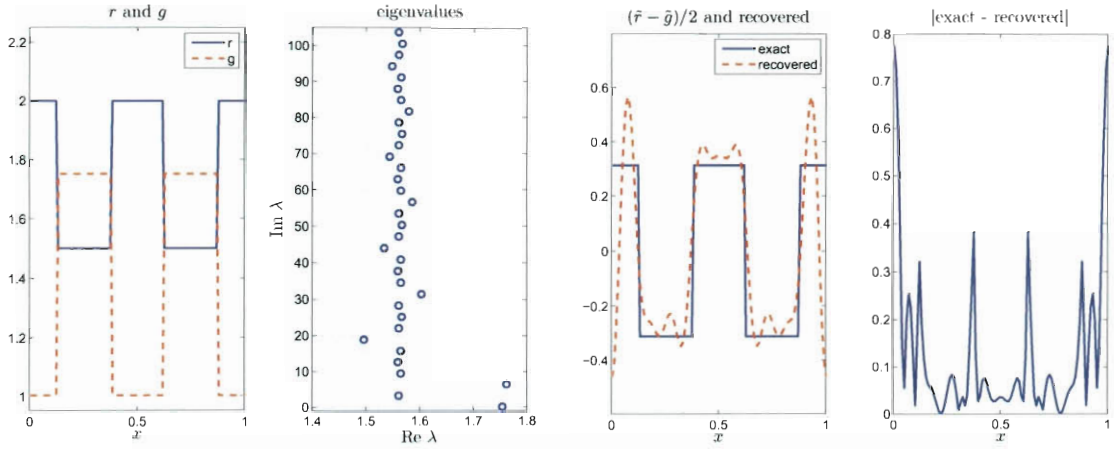

Figure 6.18 : The exact and recovered graphs to imitate a cable with two damaged intervals, with $N = 128$ and $m = 10$.

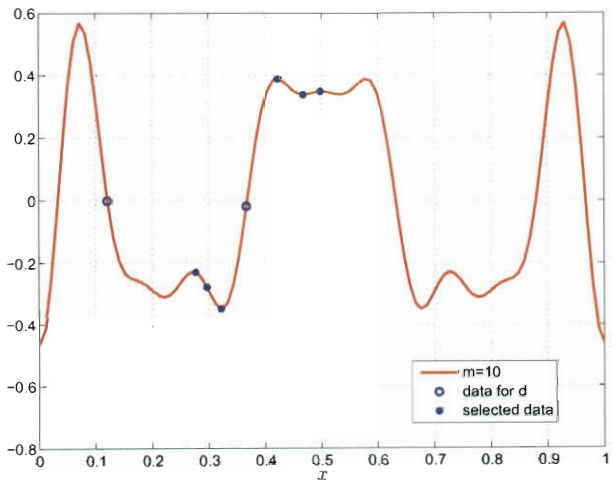

Figure 6.19 : Selected data from the recovery of $(\widetilde{r} - \widetilde{g})/2$, using $m = 10$, imitating a cable with two damaged intervals.

Chapter 7

Numerical Methods

The eigenvalues, and eigenvectors, for the forward problem

$$v'(x) + r(x)i(x) = \lambda i(x) \tag{7.1}$$
$$i'(x) + g(x)v(x) = \lambda v(x),$$

used in Chapter 6 to recover $(\widetilde{r} - \widetilde{g})/2$, were computed numerically. This chapter describes several approaches to this calculation.

7.1 Finite Differences

My first approach was a finite difference discretization of (7.1).

With N being the number of equal subintervals of length $h = 1/N$ in the discretization of $[0, 1]$ (since the assumption was made that the telegraph line was of unit length), an x vector, $[0 = x_0, x_1, ..., x_N = 1]$, was created, having $N + 1$ entries. Using this x vector, sparse diagonal matrices R and G were created for $r(x)$ and $g(x)$, respectively. To make the matrix K that would approximate the first derivative, initially the second-order accurate finite difference approximation to the first derivative,

$$f'(x_j) \approx \frac{f(x_{j+1}) - f(x_{j-1})}{2h}, \tag{7.2}$$

was used in the interior of the interval, and the first order accurate approximation to the first derivative,

$$f'(x_j) \approx \frac{f(x_{j+1}) - f(x_j)}{h}, \tag{7.3}$$

was used at the endpoints of the interval. These matrices were combined as

$$A = \begin{pmatrix} R & K \\ K & G \end{pmatrix}. \tag{7.4}$$

This matrix, A, is the starting point for the matrices for which the eigenvalues (and eigenvectors) will be calculated for the different boundary conditions.

To implement the boundary condition $v(0) = v(1) = 0$: for $v(0) = 0$ the $N + 2$ column and row were deleted from A, and for $v(1) = 0$ the $2N+2$ column and row were deleted from A to create A_1. To implement the boundary condition $v(0) = i(1) = 0$: for $v(0) = 0$ the $N + 2$ column and row were deleted from A, and for $i(1) = 0$ the $N + 1$ column and row were deleted from A to create A_2.

The results were not very accurate and each eigenvalue appeared twice. The first attempt to improve the accuracy of the results involved changing the approximation used at the end-points to a second-order accurate expression. The results produced from this code were more accurate (in that they had more digits calculated correctly) but the eigenvalues still appeared twice for both sets of boundary conditions, so another technique was attempted for the end-point calculation.

If $v(0) = 0$ and $i'(0) + g(0)v(0) = \lambda v(0)$, then $i'(0) = 0$. Similarly, if $v(1) = 0$ and $i'(1) + g(1)v(1) = \lambda v(1)$, then $i'(1) = 0$. One way to implement these boundary conditions with this discretization is by requiring $i(0) = i(h)$ and $i(1) = i(1 - h)$. This means the x vector only needs to be $[h = x_1, x_2, ..., x_{N-1} = 1 - h]$. The sparse matrices R and G were created as before. Instead of the same K for v and i, K_v (the matrix to approximate the derivative of v) is formed using the second-order accurate finite difference formula for the first derivative. Since $v(0) = v(1) = 0$, K_v is an $(N - 1) \times (N - 1)$ matrix. The matrix to approximate the derivative of i, denoted K_i, is formed by starting with a copy of K_v. Then, to enforce $i'(0) = 0$ and $i'(1) = 0$,

the (1,1) and $(N-1, N-1)$ entries are changed to be the opposite sign of the (1,2) and $(N-1, N-2)$ entries, respectively. Then, A_1 was formed by

$$A_1 = \begin{pmatrix} R & K_v \\ K_i & G \end{pmatrix}. \tag{7.5}$$

The eigenvalues MATLAB calculated from A_1 still listed each eigenvalue twice. The graphs of the eigenvectors, corresponding to the eigenvalues with smallest imaginary part (in absolute value), were plotted, and the behavior was not what was expected from the exact formulas given in Chapter 2 (spurious high-frequency oscillations occurred, not necessarily becoming better behaved as N increased) for both instances of the eigenvalue, for typical choices of N, such as 32, 64, 128, etc.

In another attempt to improve the accuracy of the results, spectral discretization was implemented in the place of finite differences.

7.2 Spectral Discretization

One way to drastically improve the accuracy of approximating a first derivative is to use spectral discretization because the same order of accuracy can be obtained with spectral discretization using a much smaller N than finite differences would require. In Chebyshev pseudospectral collocation [16], Chebyshev points

$$x_j = \frac{1}{2}\left(1 - \cos\left(\frac{j\pi}{n}\right)\right), \quad j = 0, 1, ..., N \tag{7.6}$$

are used, rather than uniformly spaced points for the x values.

The MATLAB code used to create the K matrix, which approximates the first derivative, and the x vector, is based on Trefethen's `cheb.m` code and returns the x values in descending order (from 1 to 0, instead of 0 to 1 as was programmed for the finite difference technique) [16].

The matrices R and G were formed from the x values as in the finite difference method. These matrices were again combined with the K matrix as

$$A = \begin{pmatrix} R & K \\ K & G \end{pmatrix}. \tag{7.7}$$

To implement the boundary condition $v(0) = v(1) = 0$, again the $N + 2$ and the $2N + 2$ columns and rows were deleted from A to create A_1. To implement the boundary condition $v(0) = i(1) = 0$, the first and $2N + 2$ columns and rows were deleted from A to create A_2.

Spectral discretization showed much better results compared to the finite difference technique. Only for A_1 was any eigenvalue showing up more than once; the "pure" real eigenvalue was showing up twice, even in the simplest case when $r = g = 0$. When the graphs of the eigenvectors for both of these eigenvalues were plotted, for some choices of N, both graphs, again, showed spurious high-frequency oscillations, as seen in the left graphs in Figure 7.1. However, when certain values of

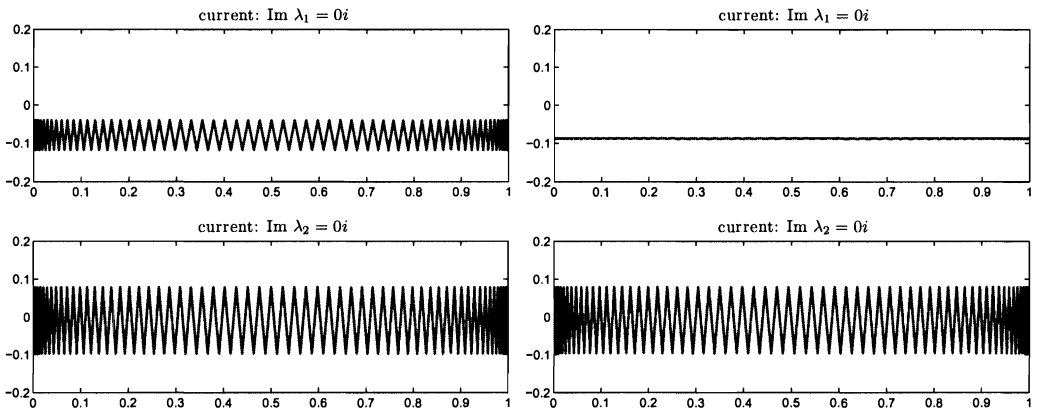

Figure 7.1 : The real part of the eigenfunction (corresponding to current) with $r = g = 0$ of the first instance of $\lambda = 0$ (top) and the second instance of $\lambda = 0$ (bottom) using spectral discretization with $N = 128$ (left) and $N = 129$ (right).

N were tried, one of the graphs of the eigenvector was close to what is predicted by the exact formulas in Chapter 2, while the other graph of the eigenvector was still showing the spurious high-frequency oscillations, as seen in the right graphs in Figure 7.1. All the other eigenvalues computed, and graphs of corresponding eigenvectors, were appropriate even when $N = 32$.

In writing MATLAB code to distinguish the valid eigenvalues from the spurious eigenvalues, first the eigenvalues and eigenvectors were calculated on a Chebyshev grid with N subintervals. The eigenvalues were sorted by their imaginary part, and the eigenvectors were sorted correspondingly. To make the following analysis simpler, the goal was to consider only the eigenvalues with non-negative imaginary part. In cases where the real eigenvalue appears twice, MATLAB may compute the eigenvalue as a conjugate pair with small imaginary part. To ensure both copies of this eigenvalue are analyzed with the rest of the eigenvalues with positive imaginary part, only the eigenvalues, and corresponding eigenvectors, with imaginary part greater than -10^{-10} were kept, resulting in val_N and vec_N. Next, the same calculation was done but on a grid of size $N/2$ (rounding up to the next integer, if necessary), resulting in $\text{val}_{N/2}$ and $\text{vec}_{N/2}$.

Then, val_N was again sorted and any entries within a chosen tolerance of the first entry of val_N were grouped together to be analyzed, with their corresponding eigenvectors. The corresponding eigenvalues from $\text{val}_{N/2}$ were also isolated with their eigenvectors.

In order to compare these eigenvectors to each other, it was necessary to interpolate the eigenvectors from $\text{vec}_{N/2}$ to have values on a grid of size N.

Then, an orthonormal basis, Q_f, for the subspace spanned by the entries from vec_N was computed. Also, an orthonormal basis, Q_c, for the subspace spanned by

the entries from $\text{vec}_{N/2}$ on the grid of size N was computed.

The goal was to analyze the angle between the subspaces spanned by the entries in vec_N and $\text{vec}_{N/2}$ for each eigenvalue. If the principle angle between the two subspaces was (nearly) zero, then the cosine of the angle would be (nearly) one. So, it was necessary to compute the singular value decomposition (SVD) of $Q_f^T Q_c$, because the singular values of the matrix are the cosines of the principle angles between the subspaces [6, p. 604].

If the singular values are within some chosen tolerance of one, the eigenvalue and eigenvector are kept. If the singular value was too far below one, the eigenvalue and eigenvector were discarded. This technique takes care of a double eigenvalue when one is valid and one is spurious, and also determines when the eigenvalue is not calculated to sufficient accuracy to be considered "converged."

With this technique, even when $N = 32$, the spurious eigenvalue was successfully sifted out, and the resulting eigenvector graphs showed what was expected, as seen in Figure 7.2.

7.3 Comparing Numerical Results to Known Formulas

After addressing the issue of spurious eigenvalues, the eigenvalues and eigenvectors calculated by MATLAB agreed with (2.6) and (2.13), the formulas for the eigenvalues for constant $r(x)$ and $g(x)$ for both boundary conditions.

Also, after sifting out spurious eigenvalues, when $r(x) = g(x)$ the eigenvalues were seen to follow

$$\sigma_k(P) = \sigma_k(0) + \int_0^1 r(x)dx, \quad k = 1, 2, \tag{7.8}$$

where $\sigma_1(0)$ is the spectrum of $\mathcal{A}_1$ when $r = g = 0$, given in (2.11), and $\sigma_2(0)$ is the spectrum of $\mathcal{A}_2$ when $r = g = 0$, given in (2.18). This relationship was proven as

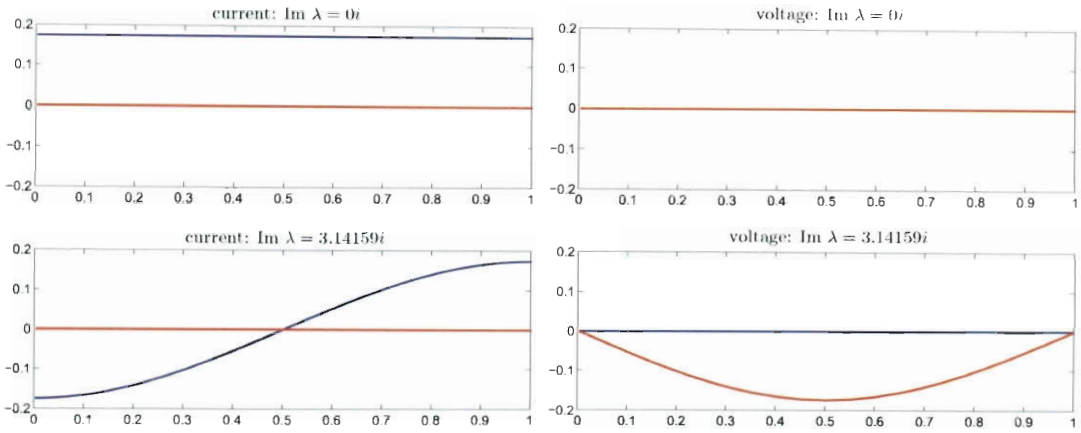

Figure 7.2 : The eigenvectors for current (left) and voltage (right) with $r = g = 0$ of $\mathrm{Im}(\lambda) = 0$ (top) and the $\mathrm{Im}(\lambda) = \pi$ (bottom) after sifting the results from spectral discretization with $N = 32$. The real part of the eigenfunction is shown in blue, while the imaginary part is red. (Notice in the graph of voltage for $\mathrm{Im}(\lambda) = 0$ the two plots are indistinguishable.)

Corollary 1.3 in Cox and Knobel's paper [4].

To illustrate this relationship, let $r(x) = g(x) = 1+0.5\sin(0.5\pi x)$, then $\int_0^1 r(x)dx = 1/\pi + 1 \approx 1.3183$. For $\mathcal{A}_1$, $\sigma_1(0) = \{in\pi\}$, from (2.11), so (7.8) predicts $\sigma_1(P) = 1/\pi + 1 + \sigma_1(0)$. Shown in Figure 7.3 in the left plot is the comparison of the eigenvalues for $\mathcal{A}_1$, when $r(x) = g(x) = 1 + 0.5\sin(0.5\pi x)$, computed in MATLAB using the spectral discretization (with $N = 128$) and from (7.8). The plot on the right shows the magnitude of the difference between the predicted and computed eigenvalues, which shows the values agree very closely.

Similarly, for $\mathcal{A}_2$, $\sigma_2(0) = \{i(2n+1)\pi/2\}$, from (2.18), so (7.8) predicts $\sigma_2(P) = 1/\pi + 1 + \sigma_2(0)$. In Figure 7.4, the left plot shows the comparison of the eigenvalues for $\mathcal{A}_2$, when $r(x) = g(x) = 1 + 0.5\sin(0.5\pi x)$, computed in MATLAB using the spectral discretization (with $N = 128$) and from (7.8). The plot on the right shows the magnitude of the difference between the predicted and computed eigenvalues,

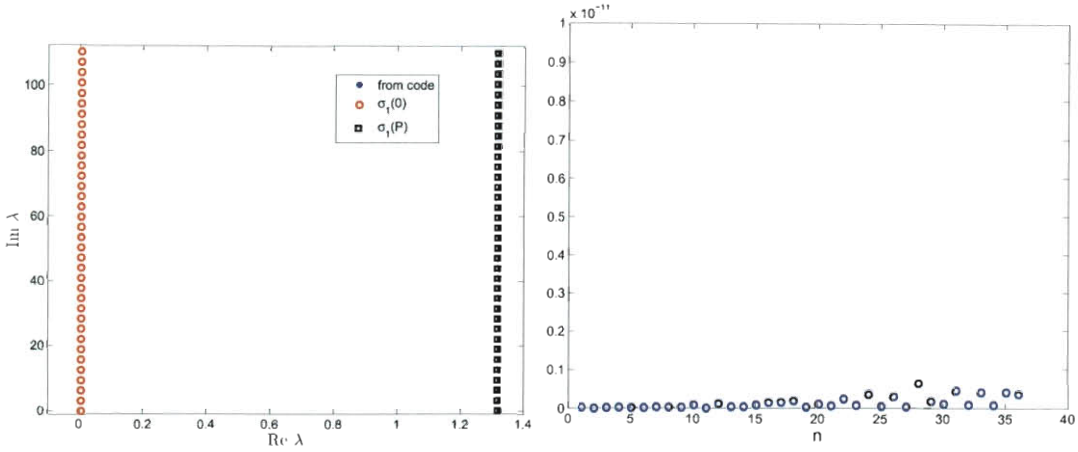

Figure 7.3 : (left) Comparison of the eigenvalues for $\mathcal{A}_1$, when $r(x) = g(x) = 1 + 0.5\sin(0.5\pi x)$, computed in MATLAB using the spectral discretization (with $N = 128$) and from (7.8). (right) Magnitude of the difference between the predicted eigenvalues, $\sigma_1(P)$, and eigenvalues computed from spectral discretization.

which shows the values agree very closely, exactly as they did for $\mathcal{A}_1$.

Included in the results reported in Chapter 6 are plots of the eigenvalues of $\mathcal{A}_1(P)$ for various choices of r and g.

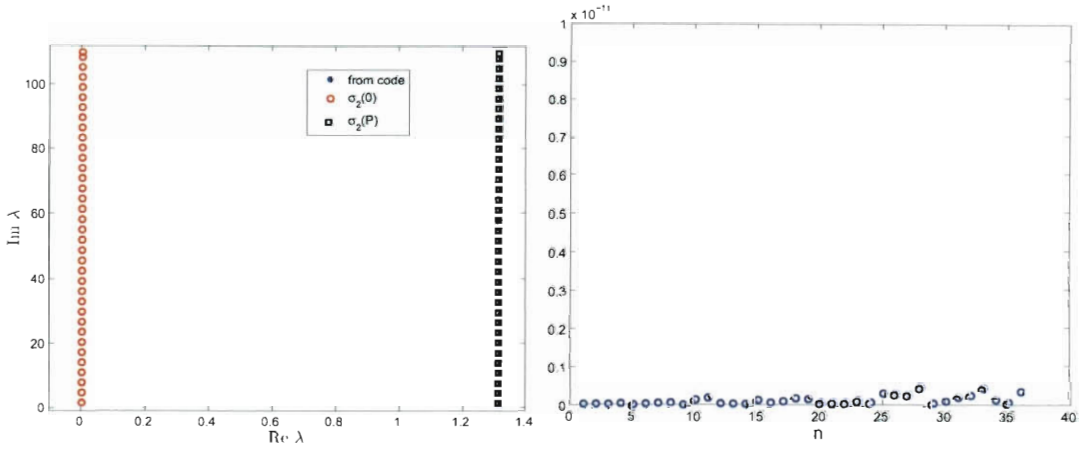

Figure 7.4 : (left) Comparison of the eigenvalues for $\mathcal{A}_2$, when $r(x) = g(x) = 1 + 0.5\sin(0.5\pi x)$, computed in MATLAB using the spectral discretization (with $N = 128$) and from (7.8). (right) Magnitude of the difference between the predicted eigenvalues, $\sigma_2(P)$, and eigenvalues computed from spectral discretization.

Chapter 8

Conclusions

The goal of this research was to refine the asymptotic expression for the eigenvalues of the operator matrix from the telegrapher's equation to accuracy $O(1/n^2)$ and use this refinement to recover information about resistance in numerical experiments.

In order to refine the asymptotic expression for the eigenvalues, first the expression for the "shooting function" was refined to $O(1/n^2)$. This refined expression enabled the refinement of the expression for the eigenvalues to $O(1/n^2)$. The steps used to refine the expression for the eigenvalues of $\mathcal{A}_1(P)$ are shown in some detail in Chapter 3. Since the procedure is almost exactly the same for $\mathcal{A}_2(P)$, the steps leading to the result for $\mathcal{A}_2(P)$ are shown in Chapter 4 in much less detail.

The procedure to use this refined asymptotic expression for the eigenvalues of $\mathcal{A}_1(P)$ to solve inverse spectral problems, specifically to recover information about resistance, is described in Chapter 5. Equation (5.7) leads to the conclusion that one of r or g can be recovered from a finite set of eigenvalues, if the other is known.

The results of implementing (5.7) for various choices of r and g for $\mathcal{A}_1(P)$ are presented in Chapter 6. When r and g are continuous, the recovery of $(\widetilde{r} - \widetilde{g})/2$ is shown to be quite accurate using only $m = 10$ eigenvalues. To present results that correlated with a submarine telegraph cable, results are also provided when r and g are discontinuous. Examples when r and g have one and two damaged intervals is presented, and the process to recover the information about the damaged intervals is described.

There are several possible directions for extending this work in the future. One possible direction for future analysis is working to understand the discrepancy between the exact and recovered ψ seen from (5.4). If ψ can be accurately recovered, then ξ can be recovered and combined with $(\widetilde{r}-\widetilde{g})/2$ to recover r and g completely. Another extension of this analysis could be to allow ℓ and c to vary in x. Also, these results could be extended for the model described by Chen et al. which involves an additional term in the telegrapher's equation described in this thesis [2].

Bibliography

[1] K. Chadan and P.C. Sabatier. *Inverse Problems in Quantum Scattering Theory, Second Edition.* Springer-Verlag, 1989.

[2] Chao-Wang Chen, Y.-W.R. Shau, and Chien-Ping Wu. Analog transmission line model for simulation of systemic circulation. *Biomedical Engineering, IEEE Transactions on*, 44(1):90 –94, 1997.

[3] S. Cox and M. Embree. Reconstructing an even damping from a single spectrum. *Inverse Problems*, 27:035012 (18pp), 2011.

[4] S. Cox and R. Knobel. An inverse spectral problem for a nonnormal first order differential operator. *Integral Equations and Operator Theory*, 25(2):147–162, 1996.

[5] S. Cox and E. Zuazua. The rate at which energy decays in a damped string. *Comm. Partial Differential Equations*, 19(1-2):213–243, 1994.

[6] G. H. Golub and C. F. Van Loan. *Matrix Computations, 3rd edition.* Johns Hopkins University Press, 1996.

[7] M. Leung, G. Dumont, G.G.S. Sandor, and J.E. Potts. Estimating arterial stiffness using transmission line model. In *Engineering in Medicine and Biology Society, 2006. EMBS '06. 28th Annual International Conference of the IEEE*, 2006.

[8] J. Li. *The Arterial Circulation, Physical Principles and Clinical Applications.* Humana Press, 2000.

[9] H. M. Lieberstein. *Theory of Partial Differential Equations.* Academic Press, Inc., 1972.

[10] P.C. Magnusson, G.C. Alexander, and V.K. Tripathi. *Transmission Lines and Wave Propagation, 3rd edition.* CRC Press, 1992.

[11] L.T. Mainardi, A. Porta, D. Lucini, M. Aquino, M. Monaco, M. Pagani, and S. Cerutti. A transmission line model for the non-invasive evaluation of the vascular mechanical properties at level of the brachial artery. In *Computers in Cardiology 1996*, pages 149 –152, 1996.

[12] J. Pöschel and E. Trubowitz. *Inverse Spectral Theory.* Academic Press, Inc., 1986.

[13] R. Redheffer and D. Port. *Differential Equations Theory and Applications.* Jones and Bartlett Publishers, 1991.

[14] T. Standage. *The Victorian Internet: The Remarkable Story of the Telegraph and the Nineteenth Century's On-line Pioneers.* Walker and Company, 1998.

[15] W. Thompson. The theory of the electric telegraph. *Proceedings of the Royal Society of London*, VII:382–399, 1856.

[16] L. N. Trefethen. *Spectral Methods in MATLAB.* Society for Industrial and Applied Mathematics, 2000.

[17] M. Yamamoto. Inverse spectral problem for systems of ordinary differential

equations of first order, I. *J. Fac. Sci. Univ. Tokyo, Sect. 1A, Math.*, 35:519–546, 1988.

Appendix A

Detailed Verification Computations

A.1 Verifying (3.7) Solves (3.8)

To verify (3.7) solves (3.8),

$$z_x(x,\lambda) = \begin{pmatrix} \left[\lambda - \frac{1}{2}\left(r(x)+g(x)\right)\right]\sinh f(x,\lambda) \\ \left[\lambda - \frac{1}{2}\left(r(x)+g(x)\right)\right]\cosh f(x,\lambda) \end{pmatrix}$$

and

$$Bz_x(x,\lambda) = \begin{pmatrix} \left[\lambda - \frac{1}{2}\left(r(x)+g(x)\right)\right]\cosh f(x,\lambda) \\ \left[\lambda - \frac{1}{2}\left(r(x)+g(x)\right)\right]\sinh f(x,\lambda) \end{pmatrix}.$$

Therefore,

$$\begin{aligned} &Bz_x(x,\lambda) + P(x)z(x,\lambda) + F(x)z(x,\lambda) \\ &\qquad = \begin{pmatrix} \left[\lambda - \frac{1}{2}\left(r(x)+g(x)\right)\right] z_1(x,\lambda) \\ \left[\lambda - \frac{1}{2}\left(r(x)+g(x)\right)\right] z_2(x,\lambda) \end{pmatrix} \\ &\qquad\quad + \begin{pmatrix} r(x)z_1(x,\lambda) \\ g(x)z_2(x,\lambda) \end{pmatrix} + \begin{pmatrix} \frac{1}{2}\left(g(x)-r(x)\right) z_1(x,\lambda) \\ \frac{1}{2}\left(r(x)-g(x)\right) z_2(x,\lambda) \end{pmatrix} \\ &\qquad = \lambda \begin{pmatrix} z_1(x,\lambda) \\ z_2(x,\lambda) \end{pmatrix}. \end{aligned}$$

So, (3.7) solves (3.8).

A.2 Verifying (3.10) Solves (3.8)

To verify that (3.10) also satisfies (3.8),

$$By_x(x,\lambda) = \begin{pmatrix} \left[\lambda - \frac{1}{2}\left(r(x)+g(x)\right)\right]\sinh f(x,\lambda) \\ \left[\lambda - \frac{1}{2}\left(r(x)+g(x)\right)\right]\cosh f(x,\lambda) \end{pmatrix},$$

so,

$$By_x(x,\lambda) + P(x)y(x,\lambda) + F(x)y(x,\lambda) = \lambda \begin{pmatrix} y_1(x,\lambda) \\ y_2(x,\lambda) \end{pmatrix}.$$

So, (3.10) also satisfies (3.8).

A.3 Verifying (3.12) Solves (3.11)

To verify that (3.12) solves (3.11), first note

$$u_x(x,\lambda) = \Phi_x(x,\lambda)\left[\int_0^x \Phi^{-1}(s,\lambda)BF(s)u(s,\lambda)ds + \begin{pmatrix} 1 \\ 0 \end{pmatrix}\right] + \Phi(x,\lambda)\left[\Phi^{-1}(x,\lambda)BF(x)u(x,\lambda)\right]$$

$$u_x(x,\lambda) = BF(x)u(x,\lambda)$$
$$+f_x(x,\lambda)\begin{pmatrix} \sinh f(x,\lambda) & \cosh f(x,\lambda) \\ \cosh f(x,\lambda) & \sinh f(x,\lambda) \end{pmatrix}\left[\int_0^x \Phi^{-1}(s,\lambda)BF(s)u(s,\lambda)ds + \begin{pmatrix} 1 \\ 0 \end{pmatrix}\right].$$

Then,

$$Bu_x(x,\lambda) = f_x(x,\lambda)\Phi(x,\lambda)\left[\int_0^x \Phi^{-1}(s,\lambda)BF(s)u(s,\lambda)ds + \begin{pmatrix} 1 \\ 0 \end{pmatrix}\right] + F(x)u(x,\lambda).$$

Therefore, on the left side of (3.11),

$$
\begin{aligned}
&Bu_x(x,\lambda) + P(x)u(x,\lambda) + F(x)u(x,\lambda) \\
&= \left[\lambda - \frac{r(x)+g(x)}{2}\right]\Phi(x,\lambda)\left[\int_0^x \Phi^{-1}(s,\lambda)BF(s)u(s,\lambda)ds + \begin{pmatrix} 1 \\ 0 \end{pmatrix}\right] \\
&+ F(x)u(x,\lambda) + \begin{pmatrix} r(x) & 0 \\ 0 & g(x) \end{pmatrix}\Phi(x,\lambda)\left[\int_0^x \Phi^{-1}(s,\lambda)BF(s)u(s,\lambda)ds + \begin{pmatrix} 1 \\ 0 \end{pmatrix}\right] \\
&\quad + \begin{pmatrix} \frac{g(x)-r(x)}{2} & 0 \\ 0 & \frac{r(x)-g(x)}{2} \end{pmatrix}\Phi(x,\lambda)\left[\int_0^x \Phi^{-1}(s,\lambda)BF(s)u(s,\lambda)ds + \begin{pmatrix} 1 \\ 0 \end{pmatrix}\right] \\
&= \begin{pmatrix} \lambda - \frac{r(x)+g(x)}{2} + r(x) + \frac{g(x)-r(x)}{2} & 0 \\ 0 & \lambda - \frac{r(x)+g(x)}{2} + g(x) + \frac{r(x)-g(x)}{2} \end{pmatrix} u(x,\lambda) \\
&\quad + F(x)u(x,\lambda) \\
&= \lambda u(x,\lambda) + F(x)u(x,\lambda),
\end{aligned}
$$

which is exactly the right side of (3.11).